



Chronology of the Upper Pleistocene loess sequence of Havrincourt (France) and associated Palaeolithic occupations: a Bayesian approach from pedostratigraphy, OSL, radiocarbon, TL and ESR/U-series data

Gilles Guérin, Pierre Antoine, Esther Schmidt, Emilie Goval, David Hérissou, Guillaume Jamet, Jean-Louis Reyss, Qingfeng Shao, Anne Philippe, Marie-Anne Vibet, et al.

► To cite this version:

Gilles Guérin, Pierre Antoine, Esther Schmidt, Emilie Goval, David Hérissou, et al.. Chronology of the Upper Pleistocene loess sequence of Havrincourt (France) and associated Palaeolithic occupations: a Bayesian approach from pedostratigraphy, OSL, radiocarbon, TL and ESR/U-series data. *Quaternary Geochronology*, 2017, 42, pp.15-30. 10.1016/j.quageo.2017.07.001 . hal-01584140

HAL Id: hal-01584140

<https://hal.science/hal-01584140>

Submitted on 22 Sep 2022

HAL is a multi-disciplinary open access archive for the deposit and dissemination of scientific research documents, whether they are published or not. The documents may come from teaching and research institutions in France or abroad, or from public or private research centers.

L'archive ouverte pluridisciplinaire **HAL**, est destinée au dépôt et à la diffusion de documents scientifiques de niveau recherche, publiés ou non, émanant des établissements d'enseignement et de recherche français ou étrangers, des laboratoires publics ou privés.

Chronology of the Upper Pleistocene loess sequence of Havrincourt (France) and associated Palaeolithic occupations: a Bayesian approach from pedostratigraphy, OSL, radiocarbon, TL and ESR/U-series data

Gilles Guérin (1), Pierre Antoine (2), Esther Schmidt (1), Emilie Goval (3), David Hérissou (4), Guillaume Jamet (5), Jean-Louis Reyss (1), Qingfeng Shao (6), Anne Philippe (7), Marie-Anne Vibet (7), Jean-Jacques Bahain (8)

1) Laboratoire des Sciences du Climat et de l'Environnement, LSCE/IPSL, CEA-CNRS-UVSQ, Université Paris-Saclay, F-91191 Gif-sur-Yvette, France;

G. Guérin (gilles.guerin@lsce.ipsl.fr),

E. Schmidt (estherdorothe.car@gmail.com),

J.-L. Reyss (Jean-Louis.Reyss@lsce.ipsl.fr),

2) Laboratoire de Géographie Physique Environnements quaternaires et actuels (UMR 8591, CNRS-Universités Paris I & Paris XII), 1 place Aristide Briand, F-92195 Meudon cedex

(pierre.antoine@cnrs-bellevue.fr)

3) Service Régional de l'Archéologie / DRAC Nord-pas-de-Calais-Picardie, 1 rue Henri Daussy, F-80000 Amiens, France (emilie.goval@culture.gouv.fr)

4) INRAP Canal Seine-Nord Europe, 16 rue du Général Leclerc, F-80400, Croix-Moligneaux and UMR 7194 CNRS, Institut de Paléontologie Humaine, 1 rue René Panhard, F-75013,

Paris, France (david.herisson@inrap.fr)

5) GéoArchÉon SARL, 30, rue de la Victoire, F-55210 Viéville-sous-les-Côtes, France (guillaume.jamet@geoarcheon.fr)

6) College of Geography Science, Nanjing Normal University, Nanjing 210023, China; Q. Shao (qingfengshao@nynu.edu.cn)

7) Laboratoire de Mathématiques Jean Leray Université de Nantes. 2, rue de la Houssinière Po Box 92208, F-44322 Nantes, France (Anne.Philippe@univ-nantes.fr, marie-anne.vibet@univ-nantes.fr)

8) Département de Préhistoire du Muséum national d'Histoire naturelle, UMR 7194 CNRS, Institut de Paléontologie Humaine, 1 rue René Panhard, F-75013 Paris, France.

(bahain@mnhn.fr),

Abstract

In connection with the future Seine-North Europe Canal (Seine-Scheldt), a large-scale rescue archaeological survey was conducted at Havrincourt (northern France) between 2008 and 2011. The discovery of several levels of Palaeolithic flint artefacts embedded in a relatively thick loess sequence (ca 6 to 7 m) preserved on a gentle slope facing North-East, resulted in a 6000 m² excavation. This opened the opportunity for a detailed pedosedimentary and interdisciplinary geochronological survey (¹⁴C, optically stimulated luminescence, thermoluminescence, ESR/U-series) that has allowed us date the sequence reliably. On the basis of these results we propose this sequence as a new pedostratigraphic and archaeological reference sequence for northern France. We present here the optical dating of the sequence performed on fine (4-11 µm) quartz grains extracted from 17 samples. The luminescence characteristics of these extracts indicate that the single-aliquot regenerative dose optically stimulated luminescence (SAR-OSL) procedure that was applied is well suited. A consistent set of optical ages was obtained for the loess deposited up to around 70 ka ago. Independent age control (pedostratigraphy, ¹⁴C, ESR/U-series dates) allowed us to apply a Bayesian approach to build a chronometric model. This in turn enabled a regional chronostratigraphic framework to be built, to constrain the correlations with neighboring regions (northern France and Belgium) and to calculate a precise age for the four Palaeolithic levels discovered, including a unique occupation related to the early Upper Palaeolithic which was previously unknown in the area.

Keywords: Loess; Palaeosols; Northern France; Optical dating; SAR; Quartz; ESR/U-series dating; Periglacial processes; Middle and Upper Palaeolithic; Weichselian

1) Introduction

Western European loess-palaeosol sequences preserve a significant terrestrial record of Quaternary history providing a window into the response of terrestrial environments to large scale Interglacial-Glacial cycles (Lautridou et al., 1985; Antoine 1994; Antoine et al., 1998, Meijs 2002, Meijs et al., 2011, Hérissou et al., 2016) and rapid climatic events during the Last Glacial (Rousseau et al., 2002, 2007; Antoine et al., 2009, 2016, Haesaerts et al., 2003, 2010; Moine et al., 2008). In northern France, these deposits have been extensively studied over the last 20 years, in parallel with numerous archaeological investigations on Palaeolithic sites (Antoine 1991; Antoine, 1994; Deschodt et al., 1998; Antoine et al., 1998, 2003a, 2003b, 2014, 2016; Lochet et al., 2002, 2003; Vallin and Masson 2003; Sellier, 2005;).

The site of Havrincourt is located at the western edge of the European loess belt near the town of Cambrai (Pas-de-Calais, France) (Fig. 1). A large-scale study of this pedosedimentary sequence was undertaken alongside rescue archaeology work within the Seine-North-Europe canal project. Between 2008 and 2010, large archaeological surveys (test-pits) were excavated down to 5 to 7 m minimal depth, locally reaching until 12 m, to detect remains of Palaeolithic occupations. This gave us the opportunity to characterize soil horizons (palaeosols) alternating with aeolian and hillwashed sedimentary deposits and periglacial phenomena (tundra gleysols and former large ice-wedge networks). The geological context and the knowledge of the regional records indicate that this sequence belongs to the last climatic cycle of the Eemian-Weichselian (Antoine et al., 1999, 2016). The sequences that were identified represent a reference for Last Glacial soil and sediment records in the north of France (Antoine et al., 2014a, 2016). In this paper we report geochronological results, including 17 optical dates obtained on fine grain quartz from the loess, along with ^{14}C and ESR/U-series dates measured on palaeontological remains. These new data are discussed in relation to other dating results (TL dates on heated flints and climato-stratigraphy) using a Bayesian approach in the context of the latest northern France loess-palaeosol chronostratigraphy. The chronological study of this site had the larger aim of providing clues to establish precise and detailed correlations with regional records in northern France and surrounding areas, and finally, to be able to connect the Havrincourt continental sequence with global palaeoclimatic records (Greenland ice and North Atlantic oceanic records).

2) Site location and stratigraphy

The Havrincourt site, located on a gentle slope exposed to the north-northeast between 80 and 110 m a.s.l., is close to an east-west dry valley belonging to the Schelde River basin. In this sector, well-developed loess-palaeosol sequences are found on white Senonian chalk and can locally reach more than 6 m thickness (exceptionally more than 10 m). Several Palaeolithic sites have also been identified (Vallin and Masson, 2003, Marcy et al., 2009).

Archaeological surveys have been carried in two different sectors, separated by about 500 m (Fig. 2) (Havrincourt 1, Hav1, in 2010 and Havrincourt 2, Hav2, in 2011), representing a total of 9 months of study and sampling over a surface of around 6000 m² to a minimal depth of 6 m (Hérisson and Goval 2013).

The occurrence of a well-preserved complex of soil and loess deposits belonging to the Weichselian Middle and Upper Pleniglacial chronoclimatic phases has produced a very

detailed record of environmental changes during this part of the Last Glacial. In addition, the topographic position of the site, coinciding with a gently sloping northeast face, favoured the trapping of loess on the leeward slope, allowing for rapid burial of artifacts and evidence for human presence. The setting up of a morphostratigraphic survey, linked to the Palaeolithic remains, was thus a central part of field investigations.

The stratigraphic survey was made both on long profiles exposed along the archaeological excavations (200-300 m long) and on some specific detailed profiles located at the places where pedostratigraphic information was the best-preserved (Fig. 2).

Chronostratigraphic and paleoenvironmental investigations were based on systematic and continuous high-resolution sampling of the main profiles (5 to 2.5 cm resolution on the 5-6 m deposit thickness according with profiles) for sedimentology (grain size, CaCO_3), micromorphology, malacology, magnetic susceptibility and soil geochemistry.

These observations and analyses allowed us to map a succession of several litho- and pedostratigraphic units represented by the following chrono-climatic succession on a synthetic stratigraphic log, from top to bottom (Fig. 3) (Antoine et al., 2014a):

Units 0 and 1 - Late Glacial and Holocene: ploughing horizon and Bt horizon of brown leached soil (top soil).

Units 2 to 5 - Upper Pleniglacial: calcareous loess and tundra gley horizons.

Units 6 and 7 - Middle Pleniglacial: boreal and arctic brown soil horizons.

Units 8 to 13 - Lower Pleniglacial: calcareous loess, tundra gley, brownish horizon and laminated colluvial deposits.

Unit 14 - Early-Glacial (EGL): grey forest soil and isohumic steppe soil horizons.

Unit 15 - Eemian: truncated Bt horizon of brown leached soil.

Unit 16 - Saalian: calcareous loess.

In addition, several horizons of permafrost features were also identified through the presence of well-developed ice wedge casts indexed from F1 to F5 (Fig. 3). Several archaeological levels including lithic artifacts in association with faunal remains have been discovered in different stratigraphic units (Fig. 4). The oldest archaeological level named Hav2- N0 (Havrincourt sector 2, level 0) is located in sedimentary unit 16. This human occupation is characterized by few artifacts but clearly shows that humans were present at Havrincourt during the Saalian stage.

Two archaeological levels were recognized within stratigraphical unit 12: Hav1-N3 (Havrincourt, sector 1, level 3) and Hav2-N1 (Havrincourt, sector 2, level 1). Two burnt flint pieces, one from each of these two levels, were dated in a previous study by

thermoluminescence to 118 ± 12 ka and 102 ± 10 ka respectively (N. Debenham, cited in Antoine et al., 2014a). No lithic refitting and no direct stratigraphic connection have been established between these levels. They may therefore potentially be two distinct human occupations. The lithic series from Hav1-N3 is characterized by the exclusive presence of large Levallois flakes, without any other element of the corresponding “chaîne opératoire”. These flakes are associated with faunal remains (n=70), mainly horse (n=13), bison (n=4) and rhinoceros (n=3). The Hav1-N3 occupation can be interpreted as a hunting site where humans used very standardized flakes both in terms of form and size. The lithic series Hav2-N1 highlights a spot of debitage in a steppe landscape turned towards the production of centripetal Levallois flakes of smaller dimensions. Horses (n=3) are the dominant faunal species recorded within this level (n=14).

Finally, unit 6a includes the Hav2-N2 occupation (Havrincourt, sector 2, level 2). It is correlated to the early Upper Paleolithic, which is rarely recorded in northern France. In this level, the objective of the lithic production is focused upon laminar products. Horse (n=21), reindeer (n=12) and bison (n=7) are the main faunal species associated with this human occupation, which is interpreted as a short-term campsite comprising activity areas dedicated both to blade production and to the exploitation of animal carcasses (n=238).

3) Geochronological studies

3a) Material and methods

Radiocarbon

Radiocarbon dating was performed on large mammal remains from archaeological layer Hav2-N2 in unit 6a and from rodent bones preserved within the infilling of the large burrows characterizing the unit 7 soil horizon (Antoine et al., 2014a).

Eight faunal remains from Havrincourt sector 2 were selected for AMS radiocarbon dating and sent to two different laboratories, the Oxford Radiocarbon Accelerator Unit (ORAU)(3 samples) and Beta Analytic (5 samples). Unfortunately, the quantity of collagen of the three samples sent to Oxford was considered to be insufficient to obtain reliable dates according to their protocol. The analyses were therefore conducted exclusively by Beta Analytic using the following procedure, requiring 2 to 10 g of bone. The sample was dissolved in dilute acid to eliminate apatite and carbonate, to determine the quality of the remaining ‘collagen’. If the quality was acceptable, the sample was then washed in NaOH in order to remove exogenous organic contaminants. This step usually destroys part of the ‘collagen’ but enables a clean sample to be obtained for radiocarbon analyses. After a final acid washing, the remaining

'collagen' was dried and the $^{13}\text{C}/^{12}\text{C}$ ratio determined. If the result was acceptable, the ^{14}C dating analysis was performed. In the case of the Havrincourt bones, the application of ultrafiltration was not requested.

Optically stimulated luminescence (OSL)

A set of 17 samples was extracted from eight pedosedimentary units from the Havrincourt 1 (Hav1) and Havrincourt 2 (Hav2) sites. Sampling points were carefully chosen for their stratigraphic positions and restricted to those showing a good visual homogeneity of the surrounding sediment and no evidence for post-depositional disturbances or diagenesis. Sampling was undertaken using copper tubes (35 mm diameter, 140 mm length) introduced horizontally into the sediment. After extraction they were sealed at both ends to prevent exposure to light. The sampling locations are shown in Figure 5. For dosimetry purposes, about 2 kg of the sediment surrounding the OSL tube was removed and averaged to be representative of a 30 cm diameter zone.

Luminescence analyses were performed on polymineral fine (4–11 μm) grains extracted from the inner material of the sampling tubes of which both ends have been discarded. Sample preparation techniques have been performed using usual procedures (Lang et al., 1996; Frechen et al., 1996). Organic matter was eliminated using a hydrogen peroxide treatment (40%, 24 h) then quartz grains were isolated by etching for 5 to 12 days in hydrofluorosilicic acid (H_2SiF_6) followed by rinsing in hydrochloric acid (3N, 5 h). Aliquots were prepared by settling of a 1 mg/ml suspension on 10 mm diameter stainless steel discs. Final quartz deposit is about 1 mg/cm^2 . All luminescence measurements were performed using a Risø TL/OSL-DA-15 system equipped with blue (470 nm) light-emitting diodes and an IR (830 nm) laser diode (Bøtter-Jensen et al., 2002). The luminescence signals were detected through a 7.5 mm thick Hoya U-340 filter.

Each quartz fraction was checked for purity by an IR-test on three discs (regenerative dose of ca 20 Gy, preheating at 260 °C for 10 s, IR-stimulation at 50 °C for 40 s, blue-light simulation at 125 °C for 40 s). For all samples, the sensitivity to infrared stimulation was close to or less than 1% of the corresponding OSL signal, much lower than the 10% generally accepted (Vandenbergh 2004), and the IR depletion ratio (Duller 2003) deviated less than 1.5% from unity.

Irradiations were performed with the $^{90}\text{Sr}/^{90}\text{Y}$ source of the TL-OSL reader. Its dose-rate on 01/01/2008 is 0.153Gy/s and has been calibrated using fine grains quartz deposits in the same conditions as OSL measurements. This calibration uses a ^{137}Cs gamma source as reference

(Guérin and Valladas, 2014). Alpha efficiency factors were measured using an alpha irradiator equipped with a 3.7 MBq ^{241}Am source with an 8 mm diameter emission surface emitting $7.68 \cdot 10^5$ alpha/cm²/s. Sample irradiations were performed in a vacuum chamber (in order to preserve an incident energy for the alpha beam of about 5.2 MeV) using 6 mm diameter discs with a close to 1 mg/cm² sample deposit.

The luminescence determination of the equivalent doses was achieved using a single-aliquot regenerative-dose (SAR) procedure (Murray and Wintle, 2000). All samples have similar OSL behaviour. The OSL signal shows a 90% decrease of the signal in less than 1.1 s (Fig. 6). The signal has been integrated on the first 2 seconds of stimulation minus the background determined on the interval 33-35 s. The total blue stimulation is 36.7 s at 125 °C and 90% of blue LED power (ca 20 mW/cm² based on manufacturer's information). Each measurement was followed by a test dose of 10 Gy and cutheat at 180 °C for 1 s. The OSL measurement (Tx) gives the corrected OSL signal L_x/T_x .

Parameters of the SAR protocol were fixed individually for each sample. The preheat temperature is chosen when the following 3 conditions are met. First, satisfaction of the preheat plateau test. This test was performed for all the samples for preheat temperatures ranging from 180 °C to 320 °C with a 20 °C step (Fig. 7). The detailed protocol is summarized in Table 1. The second condition is the value of the recycling ratio that must be close to unity (within a few percent). The last is the fulfilment of the dose recovery test (Murray and Wintle 2003). For 8 samples, the determination of the value for preheat temperature was achieved using an additional "preheat recovery test" where, as for natural signal, the given dose is measured for preheat temperatures ranging from 180 °C to 320 °C with a 20 °C step. We performed the dose recovery test by bleaching our sample with blue LEDs (ca 20 mW/cm²) at 125 °C for 600 s. Since its introduction, it has been noted that the dose recovery test may depend on the way the sample is bleached, or for some other reason, and may not be universal (Wang et al., 2011). We checked this aspect on five samples by bleaching the OSL signal using a solar simulator (3 h exposure at 5 cm with a 250 W Osram-Powerstar HQI-T). They showed no difference in the recovery test. Other tests were done on some samples as follows. Without bleaching of the natural signal, some aliquots were irradiated with a test dose Δ and then measured by SAR. The extrapolated dose of these aliquots D_{add} should be equal to the sum of the test dose Δ and the extrapolated dose D_e of natural sample aliquots. This test can be expressed by the ratio $(D_{\text{add}}-D_e)/\Delta$ that must be close to unity. Doing this prevents some unanticipated influence of bleaching in determining the recovery dose

and can be done at the same the preheat temperatures used in the plateau test for which the SAR equivalent dose is measured.

The determinations of the SAR equivalent doses were done using the growth curve as shown in Fig. 6. The average values and their standard errors (it must be multiplied by 2.12 to get the 95% confidence interval) are reported Table 2. For each sample, equivalent dose is measured on nine aliquots as well as the dose recovery value.

It can be noted that the preheat temperature differs slightly from one sample to another and lies between 250 °C and 280 °C a range where both the recycling ratio is close to 1 and equivalent dose is not dependent on temperature as in Fig. 7 The more frequent value is 260 °C.

For all aliquots (equivalent dose, recovery dose, etc.) this curve is best fitted with the sum of a saturating exponential and a linear term function (Wintle and Murray, 2006). Calculation of the extrapolated dose has been computed without taking into account the recycling point. This calculation is achieved by using data analysis software developed in our laboratory. The growth curve model is fitted to the experimental data using a Levenberg-Marquardt algorithm, giving the same weight to each data point. The example in Fig. 6 (HAV2 P5-4) is representative of the luminescence characteristics exhibited by our samples. All samples have a natural signal that intersects with the beginning of the linear region of the growth curve; this corresponds to a dose level where saturation is sufficiently low to allow interpolation. It can be noted that curves of natural and regenerated OSL signals have the same shape and are indistinguishable.

The dose recovery experiments indicate that the SAR protocol is able to measure within 4% a laboratory dose given prior to any heat treatment. These criteria and the fulfilment of the usual tests provide strong evidence for that the samples are suited for dating with the SAR protocol.

Annual dose rates were determined using U, Th and K concentrations of the sediment, its water content and an estimate of the cosmic contribution. These concentrations were measured on a sample representing a zone of ca 30 cm of sediment around the OSL sample as described above. Prior to gamma spectroscopy, the sediment was dried (3 days, 105 °C). Around 10 g of sample was kept at least a week in a sealed tube (100 mm, 15 mm diameter). Measurements lasting ca 24 h. were performed in the *Laboratoire Souterrain de Modane* (CNRS-CEA) where the influence of cosmic rays is drastically limited. We used a very low background GeHP detector whose gain is calibrated with the AIEA standards (RGTh and RGU) for U and Th families and a KCl reference for K activity. Concentrations are

summarized in Table 3. Standard errors (1σ) quoted in this table reflect the counting statistics with no appreciable contribution of the AIEA standard uncertainties (IAEA 1987). Within the precision of the gamma measurements the mass activities of the elements of the U and Th decay chains show that all samples are in radioactive equilibrium (for detailed radionuclides activity see supplementary Table 1). Concentrations of U, Th and K were calculated using the specific activities of ^{234}Th , ^{228}Ra and ^{40}K respectively.

To quantify the effect of moisture on the annual dose rates we used the water saturation content (Aitken 1985). This parameter has been measured (Table 3) for each sample. A batch of ca 50 g is soaked in water for over 24 h, then drained for ca 6 hours (wet weight) checking when the weight is stabilised, then the batch is dried for 1 day at 105 °C (dry weight). Saturation content is the difference between the wet weight and the dried weight divided by the dried weight. Incidence of moisture is calculated by assuming the mean water content of the sediment since its deposition lies between 60 to 100% of the saturated value determined in the laboratory. We further assume this mean has a uniform distribution in this interval, thus following the recommendation of the Joint Committee for Guides in Metrology (JCM100 2008; §4.3.7). This can be represented by the factor 0.80 ± 0.12 ; the associated uncertainty being compatible with the Gaussian error propagation law. This method, using saturation content, has been preferred because the natural water content could not be determined reliably for all the samples as some were not properly sealed on the field.

Alpha radiations having a reduced luminescence effectiveness (Aitken 1985), an a -value for each sample was determined as follows. The L_x/T_x obtained after a calibrated alpha irradiation was compared to the L_x/T_x obtained after a calibrated beta irradiation (test dose for T_x and preheat parameters being the same as those of the SAR protocol). The alpha particle flux intercepted by the sample delivers a dose to the sample. The alpha dose rate of the source is calibrated for the fixed geometry of irradiation described in the introduction of this chapter. Initially calibration uses the number of particles by seconds and has been converted into a radiation dose (0.1134 ± 0.0028 Gy/s) that includes small corrections for particles inclinations and incident energies (Guérin, 1982; Valladas and Valladas, 1982; Aitken 1983, 1985). Eventually, the sample deposit density was checked and corrections to the a -value were applied when the density differs from 1 mg/cm^2 .

The measured a -value varies from 0.039 to 0.045 (Table 3) with a mean of 0.042; close to the 0.039 a -value mean determined by GLSL (green light stimulated luminescence) on fine grains quartz extracts from sediments (Rees-Jones and Tite 1997).

Annual dose rates were calculated using data in Tables 2 and 3 and the last revised conversion factors (Guérin *et al.*, 2011). The contribution of cosmic rays to the dose rate was calculated using the depth from the surface (Table 3) and a sediment density of 2 (Prescott and Stephan 1982; Prescott and Hutton 1994).

ESR/U-Series dating

Two horse teeth found in two different archaeological levels (units 6a and 12 respectively) were sampled for ESR/U-series analyses. The teeth were analysed according to the protocol and parameters described in Bahain *et al.* (2015) (Table 4).

Enamel layers have been separated then cleaned with a dental drill in order to eliminate any contamination and the external alpha contribution. The thickness of the removed part on each enamel side (Table 4) has been taken into account in the beta contribution calculation (Brennan *et al.*, 1997). The enamel sample was then ground and sieved, and the 100-200 μm fraction was split into ten aliquots. Nine of them were irradiated using a ^{60}Co gamma source (CEA Saclay, France) at the following doses: 34, 55, 85, 137, 228, 3271, 586, 937 and 1475 Gy. ESR intensities (I) of the ten aliquots were then measured using a Bruker EMX ESR spectrometer and equivalent doses D_E were extrapolated from the experimental data using a single saturation exponential function (Duval and Grün 2016) with Microcal *Origin Pro 8* software (weighting by $1/I^2$).

Uranium content of the dental tissues (without any preparation) was estimated by gamma spectrometry measurements using a low background GeHP gamma detector (for 1 to 8 days according to the amount and activities of the considered samples) at the *Muséum National d'Histoire Naturelle* at Paris, France. The tissues were then analysed by U-series using a Neptune MC-ICPMS device at Nanjing Normal University, China following the chemical protocol of Shao *et al.* (2015). Eventual Ra and Rn losses from the dental tissues were also estimated from cross-checked gamma and ICP data (Bahain *et al.*, 1992).

Activities of natural radionuclides from associated sediments were also determined by gamma spectrometry (usually with measurements for a couple of days) and *in situ* gamma measurements were performed in the two dated levels (6 and 3 measurements for US6 and US12 respectively) using a Canberra Inspector 1000 spectrometer by the threshold technique (Mercier and Falguères, 2007). Data obtained from the two sets of measurements (including for OSL samples gamma dosimetry) are very homogeneous for each dated level. As for OSL, annual dose rates were determined using U, Th and K concentrations of the sediment directly

associated with the tooth samples on 100 g sediment boxes in a similar manner to that used for OSL samples. The water contents determined during the OSL study for the sediments from the two considered units were used for the age calculation. As for the OSL study, the contribution of cosmic rays to the dose rate was calculated using the depth from the surface and a sediment density of 2. Annual dose rates were calculated using an alpha efficiency (k-value) of 0.13 ± 0.02 according to Grün & Katzenberger-Appel (1994) and the last revised conversion factors (Guérin *et al.*, 2011).

4) Results

Radiocarbon

The ^{14}C results obtained for the eight analysed samples of Havrincourt are given in Table 5 (calibrations according to IntCal13 curve; Reimer *et al.*, 2013). Concerning the samples carried out from the archaeological level Hav2-N2, only two bones provided dating estimates, the other analyses failed due to low collagen yields. The ^{14}C ages of these two samples are 27020 ± 140 BP and 28100 ± 180 BP and they therefore place this Upper Palaeolithic level into the late Aurignacian or early Gravettian periods, despite the absence of typical pieces in the lithic assemblage.

Several rodent bones samples recovered in burrows of unit 7 were also dated by ^{14}C at 40100 ± 370 BP and 42090 ± 380 BP, i.e. between 43 and 46 ka cal BP. This age postdates the unit 7 sediment deposition and corresponds to a period of climatic improvement prior to the cold event represented by the F5 ice wedge formation.

OSL

Table 6 shows the optical ages of different Havrincourt profiles from the two sectors. The first, HAV1 P1, is dated at high resolution using 10 samples distributed on the profile. Ages span from 67.6 ± 3.9 ka to 28.9 ± 1.9 ka. Above the HAV1-P1-7 sample, all ages obtained are in good accordance with stratigraphic order. As fossilised burrows are frequent in this zone, the underestimated age of HAV1-P1-7 could be explained by an *in situ* contamination due to the occurrence of a burrow filled with younger sediment.

Five ages have been measured in the HAV2-P5 profile. They span the interval between 61.7 ± 4.0 and 28.4 ± 1.8 ka. As for the HAV1 profile, they follow the expected stratigraphic order. In this profile, two ^{14}C ages have been measured on 2 mammal bones from the Hav2-N2 archaeological level corresponding to HAV2-P5-4. In Unit 6a, the OSL age of 34.9 ± 2.3 ka is

in agreement with the ^{14}C ages (27020 ± 140 BP and 28100 ± 180 BP), indicating that the parameters used in the SAR protocol and for dosimetry calculations lead to age determination with no major bias. Evidence for small bias is given by the ^{14}C age (ca 46 ka calibrated) of marmot and gopher skeletons found in burrows from unit 7, which are younger than the HAV2 P5-5 age (51.5 ± 3.2 ka) located at the top of unit 7.

ESR/U-Series

Table 7 shows the calculated ESR/U-series ages (US model, Grün et al., 1988 and AU model, Shao et al., 2012), various dose-rate contributions and the uranium uptake parameters for each tooth. The choice of the U-uptake model that was applied is not arbitrary, but constrained by the analytical data (isotopic ratios, D_E and d_a) and restricted to only one model. The dose conversion factors of Guérin et al. (2011) and a water content of $33 \pm 4\%$, corresponding to the values determined on OSL samples, was used for the age calculation. The results are 34.0 ± 2.0 ka and 67.0 ± 4.0 ka for archaeological levels Hav2-N1 (unit 6a) and Hav2-N2 (unit 12) respectively and are in agreement with corresponding OSL HAV2-P5-4 and HAV1-P1-9 ages.

5) Bayesian treatment

In order to provide a more informed and robust view of the chronology of the sequence, a Bayesian hierarchical model was built with *ChronoModel* software (version 1.5) (Vibet et al 2016). *ChronoModel* is free software that is intended to provide tools for constructing chronologies in archaeology from several dating results (^{14}C , OSL etc) and temporal constraints (Lanos et al. 2015, 2017).

The Event model combines dates that are assumed to be contemporaneous by introducing an error term that may correct for unknown errors:

$$t_i = D + \epsilon_i, \quad (\text{Eq. 1})$$

where ϵ_i represents the error that might exist between the date t_i obtained from the archeometric method and the date of interest D . The distribution of ϵ_i is a Gaussian distribution with zero mean and variance σ_i^2 . The choice of a symmetric distribution is justified by the fact that the date t_i may be older or younger than the date of interest (See Lanos and Philippe 2017).

Modeling

The aim of the modeling is to obtain precise ages for the Paleolithic levels and the period of deposition of the associated geological layers. The observations used for these estimations are the date estimates obtained from the different dating techniques and the stratigraphic order, which forms the basis of the prior information for the model.

At Havrincourt, the chronology is mainly based on OSL measurements. 17 OSL samples were taken from two different sectors and from several units (from unit 12 to unit 2) that were observed in both sectors. The OSL age corresponds to the date of the last exposure to the light of the quartz grains, so it refers to the deposition time of the different units. In the modeling with *ChronoModel*, each event is associated to only one OSL measurement, and the event date is the last exposure time of the sample to light. All events from the same layer are gathered in a phase in order to estimate the period of deposition of the associated layer. Hence, 8 groups of dates were defined in the Havrincourt sequence, corresponding to 8 dated units at the site (Table 6 and Figure 8). Moreover, temporal order can be imposed between these events taking into account the geological and the pedostratigraphic information (Figure 8).

Other samples were collected and dated from the site (Tables 5 and 7) as mentioned above: two horse teeth from Units 12 and 6a dated by ESR/U-series and mammal bones (Units 7 and 6) dated by radiocarbon. These dating techniques date the death of the animal that lived on (for the horses) or into (for the rodents) the sediment in which they were found. According to geological and pedostratigraphic information, these dates comprise prior information, and are included in the model as *Terminus Ante Quem* / *Terminus Post Quem* (Figure 8). In addition, we consider that the two TL dates constrain US12 as two *Termini Post Quem*. These TL dates can therefore be older than the estimated date of the start of US12.

Computational aspects

Markov Chain Monte Carlo (MCMC) algorithms are implemented to approximate the posterior distribution of the dates. To assess the agreement between the posterior distributions and the numerical approximations, three Markov chains were run in parallel. For each chain, 1 000 iterations were used during the Burn-in period, 20 batches of 500 iterations were used in the Adapt period, 100 000 iterations were drawn in the Acquire period but only 1 out of 10 were kept in order to break the correlation structure.

From the analysis of the history plots, all Markov chains reach their equilibrium before the Acquire period. This is confirmed by the Gelman-Rubin criterion. Indeed it is equal to 1 (this is the expected value to confirm that all of the Markov chains reached equilibrium). The

autocorrelations of the three Markov chains are not significant, meaning the rate of subsample (1 over 10) is enough. We generated acceptable samples for the posterior distribution. Gathering the three chains, a total of 30 000 iterations was collected in order to give reliable estimations of the posterior distribution for each parameter.

Results

The Bayesian chronological approach implemented in *Chronomodel* is based on a hierarchical classification called “*event model*” (see Lanos and Philippe (2017) for the description of the model) The main idea is to embed all the dates in “*event model*” to allow individual errors between the target date and the dates obtained by different chronometric techniques.

The main interest of this approach is to provide a robust model with respect to outlier dates (dates that are not properly related to the target date) or temporal order inversions. To assess the suitability of the model, we analysed the posterior distributions of the standard deviations of these error terms. For all of the dates, the maximum *a posteriori* probability estimate is smaller than 2,000 years. These small values (with respect to the estimated ages, between 20,000 and 130,000 years) indicate the good fit between the model and the data.

In Figure 9 we show the posterior distributions of the minimum and maximum of each group of dates defined in Figure 7 and corresponding to the different stratigraphic units. The minimum and maximum values provide an estimation of the beginning and end of the sediment deposition of the unit associated with the group of dates. Only one date is associated with the Hav2-N1 archaeological level, US10 and US5. So, for these three levels, the minimum and the maximum are equal.

In Figure S1 the supplementary information is shown which characterizes the different periods. The *time range interval* (Philippe *et al.* 2017) gives an estimation of the period taking into account the uncertainty on the estimation of the beginning and the end. More formally, it corresponds to the shorter interval covering all the dates of the group with 95% probability. The numerical values are summarized in Table S2.

The whole data set is stratigraphically coherent. We can observe, however, that for the probability distributions associated with layers US2 and US12 (Figure 9), heavy tails are present due to the lack of prior information for these two periods. Unlike other units, there is no temporal constraint on the beginning of US12 and the end of US2. For the HAV2-N1 archaeological level, the age of the analyzed tooth is coherent with the estimated end of deposition of the US 12 sediments, between 74.0 and 61.4 ka, and differs greatly from the flint TL ages. On the other hand, the dates obtained on Hav2-N2 paleontological material are

in agreement and provide an interval ranging between 37.0 and 30.4 ka. Lastly, the range derived from the ^{14}C dates of the rodent remains from US7 and from overlying and underlying sediments (US7 and US6, including Hav2-N2 archaeological level) place the deposition of these units during MIS3 as well as during the development of the F5 ice wedge stage.

6) Chronoclimatic interpretation of the sequence and regional comparison

The geochronological data obtained at Havrincourt allows us to consider how the sequence compares to the global chronoclimatic subdivisions recently proposed for the Last Glacial loess sequences of northern France and Belgium by Antoine et al. (2016)(Fig. 10)

Eemian Last Interglacial and Early-glacial (LPG)

The Weichselian Early-Glacial corresponds to the time interval between the end of the Last Interglacial (Eemian) and the Lower Pleniglacial starting at about 70 ka with the first typical loess deposition. In western Europe, and especially in northern France, the analysis of numerous Early-glacial soil complexes has shown two periods of different duration: A) a long grey-forest soil phase and B) a short steppe soil phase.

Phase A (MIS 5c to 5a) starts with a first event of erosion and colluvial deposition during the first cold stage directly following the Eemian ($\text{MIS } 5\text{d} \pm 112 \text{ ka}$). These colluvial clayey-silty deposits are then affected by a pedogenesis (BSO Soil) that shows an intermediate facies between the Interglacial Bt horizon and a grey forest soil (Bth). The characteristics of this horizon include clayey to silty-clayey weakly humic stratified coatings, and numerous earthworm bioturbation features, corresponding to a continental climate, which is comparable to that of present-day central Europe. A deep seasonal freeze episode then impacted this horizon during the cold stage at the transition between MIS 5c and 5b (~ 90-88 ka). This episode is followed by the deposition of silty-clayey colluvial deposits reworking the underlying soil horizons in which a new and markedly more humic grey-forest soil pedogenesis develops. This horizon (soil SS1), exhibiting numerous earthworm galleries and chambers, testifies to upbuilding (cumulic) soil formation dynamics during MIS 5a. The SS1 soil is then impacted by a deep seasonal frost event and a strong erosional event during the very intense climatic deterioration that marks the end of MIS 5a around 78 ka ago (GS 21).

Phase B (end of MIS 5a ~ 78-70 ka ago) is represented by the formation of isohumic soils (Ah horizons) indicating a markedly more arid environment that is typical of a more arid

steppe landscape. This part of the complex (soils SS2 and SS3a&b) is clearly distinguished by the occurrence of the first aeolian deposits. It corresponds in all probability to an expanded response of the continental environments to the short climatic oscillations observed in the Greenland Ice cores between ~ 75 and 70 ka ago (GI 20 and 19).

At Havrincourt, the record of the impact of these complex climatic variations is not well preserved and is restricted to unit 14 including only a grey forest soil horizon (unit 14b) and an isohumic soil horizon (14a) overlying the truncated Eemian palaeosoil (unit 15).

Weichselian Lower Pleniglacial

Given the OSL and ESR/U-series dating results, field observations (significant erosion, colluvial facies, frost cracks) and sedimentology data (showing increasing wind dynamics), Havrincourt units 13 to 8 are allocated to the initial phases of the Weichselian Lower Pleniglacial and correlated to MIS 4. Unit 13 corresponds to heterogeneous bedded colluvial deposits related to a significant erosion of the former levels including the early-glacial humic soil complex. Even if this unit were not dated in the present work, its geological location in the sequence, by comparison with the other regional records, places its deposition during the Lower Pleniglacial. Above it, the homogeneous and mainly non-calcareous brown silt of unit 12 (*Havrincourt brown silt*, HBS) incorporates a strong aeolian component and has been dated to ca 70 ka ago. However, OSL ages of 67.6 ± 3.9 ka and the ESR/U-series age of the tooth recovered from the HAV2-N1 archaeological layer (67.0 ± 4.0 ka), are clearly in agreement with an allocation to Lower Pleniglacial, which is also strongly suggested by the results of the Bayesian model.

The top of the Havrincourt brown silt is marked by the development of a very thin hydromorphic horizon (micro-gley) related to the increase of surface moisture and to freeze-thaw processes, then by the deposition of loessic material poor in CaCO_3 (unit 10). After another gley sediment recorded in unit 9, aeolian sedimentation is reinforced by the deposition of a loess deposit showing a constant thickness in all profiles at Havrincourt (unit 8), which reflects a significant increase in wind dynamics and a more advanced and intense cold phase with the sedimentation of the first typical carbonated loess of the Last Glacial period ca 60 ka ago.

There are numerous similarities between this part of the Havrincourt sequence and other French and Belgian records (Fig. 10), in which the Early-glacial soil complex is overlain by heterogeneous stratified silts and soil lenses capped by a homogeneous brown horizon known as the *Malplaquet Soil* (Haesaerts et al., 1999, in press). The first evidence of loess

sedimentation in these sequences always appears above this brown horizon and could correspond to the calcareous loess dated at ca. 65 ka at Harmignies and Nussloch (Antoine et al., 2001; Frechen et al., 2001).

Weichselian Middle Pleniglacial

At Havrincourt, as in numerous Northern France loessic sequences, the uppermost Lower Pleniglacial loess is affected by a total decalcification linked to the development of a boreal brown soil, corresponding to a Bw horizon of boreal brown soil (Cambisol / unit 7). The available dates confirm it belonging to the lower half of the Middle Pleniglacial. This brown soil is characterized by numerous large rounded or oval bioturbations (krotovinas: 5 to 15 cm in diameter) at the site resulting from burrowing by small mammals (marmots, ground squirrels, Arvicolidae, steppe polecat). The large mammal assemblage found in this horizon includes large herbivores such as horse, woolly rhinoceros and mammoth (Antoine et al., 2014). According to ^{14}C ages obtained from rodent bones from krotovinas, the surface of the soil where these mammals have been living is dated at about 42-46 ka BP.

A first network of large V-shaped frost cracks of the ice-wedge type (≈ 1.5 m deep) then opens at the top of this soil horizon (F-5). The formation of the upper part of the *Havrincourt soil complex* (unit 6) begins with a new thin loess deposit mostly trapped in the ice-wedge casts of the F5 level. This is followed by at least two phases of soil formation corresponding to a hydromorphic arctic brown to arctic meadow soil horizon, strongly structured by the freeze-thaw processes connected with the ice-wedge level F-4. Given the available dates, the Upper Palaeolithic human occupation Hav2-N2, preserved in its upper part, could therefore date to ca 31-32 ka ago. The early Gravettian cultural attribution of the associated lithic industry seems supported by the recent discovery 70 km southwestwards of the Renancourt-1 site, close to Amiens, which contains a similar industry in association with several female figurines (“Venus”) in chalk. This was dated by OSL and ^{14}C to ~27-28 ka cal BP (Antoine et al., 2014b), in the same time range as the Havrincourt Hav2-N2 level.

Weichselian Upper Pleniglacial

Overlying this brown soil complex are sediments dating to the Upper Pleniglacial. This is evidenced at Havrincourt and in the wider regional profiles by a marked acceleration of loess sedimentation rates. A tundra gley (unit 5) is the first unit allocated to this period. The formation of this horizon results from seasonal water saturation of the active layer of a

permafrost indicated by its connection with the large ice-wedge casts of the main network (F-4). Our results date the tundra gley formation to ca 31 ka ago.

Later, the fossilization of this horizon and of the network of large ice-wedge casts indicates that loess deposition occurs in a dry and cold environment. The peak of this first loess unit of the Upper Pleniglacial is underlain by a thick and complex tundra gley (unit 3) which is subdivided into two horizons separated by a thin bed of calcareous loess, mainly preserved within an ice-wedge cast (network F-3). The infilling of this F-3 network shows local laminations and cross stratification indicating a phase of intense permafrost thawing during an episode of interstadial warming (Antoine et al., 2014a).

The upper horizon of the tundra gley is associated with a large ice-wedge cast network with homogeneous loess (unit 2) infilling $\approx 0.3 \times 1.2$ m deep (network F-2), systematically superimposed on the previous level (F-3). As there is not upper constraint for this unit 2, the Bayesian age estimate for the range is quite large but the OSL date (28.4 ± 1.8 ka) available from this loess shows that this part of the sequence accumulated very rapidly, possibly over a span of ca. 2 to 3 ka at the most, between 26-27 and 28-29 ka ago.

6) Conclusions

The OSL, ^{14}C , TL and ESR/U-series results from Havrincourt represent the first reliable set of dating results for the Upper Pleistocene loess-palaeosol sequences of northern France. The Bayesian modelling allows us to test the reliability of the dates and age estimates with respect to the stratigraphic constraints. The following observations can be drawn:

- For the first time, evidence has been found for the deposition of a typical calcareous loess bed during the Lower Pleniglacial at about 70-65 ka ago.
- Accurate dating of the youngest brown soil horizon (arctic brown soil) marks the end of the Middle Pleniglacial by ca 38-33 ka BP, as it does for all European loess sections,
- Evidence has been obtained for the deposition of a very homogeneous calcareous loess bed during the major climatic degradation (centered on 30.5 ka BP) in the reference palaeoclimatic records from Greenland and North Atlantic marine cores. This suggests that the Heinrich 3 event is coeval to the onset of a major climatic modification in the European continent, in terms of wind regime and land erosion.
- Accurate dates have been obtained for a first succession of permafrost events each marked by the formation of large polygonal networks of ice-wedge casts with pure loess infilling between 26 and 29 ka BP.

- We obtained dates for four levels of human occupation including an Upper Palaeolithic level through the ^{14}C dating of large mammal bones and ESR/U-series dating of large mammal teeth.

In the near future, a new rescue archaeological campaign planned on the area of Havrincourt and in the surrounding loess zone crossed by the Seine-Nord-Europe Canal Project will allow us to refine these results and provide new data for loess and Palaeolithic research in western Europe.

Acknowledgements

The authors thank the French Institute for Rescue Archaeological Research (INRAP Nord-Pas-de-Calais-Picardie / Coordination Canal Seine Nord-Europe) for the financial support to OSL and ESR/U-series dating of the Havrincourt sequence. We thank also gratefully two anonymous referees and Tom Higham, QG editor, for their constructive comments, helps in English writing and proposals that are allowed to improve greatly the manuscript.

References

- Adamiec, G., Aitken, M., 1998. Dose-rate conversion factors: update. *Ancient TL*, 16, 37-50.
- Aitken, M.J., 1983. Alpha particle effectiveness: numerical relationship between systems. *Ancient TL*, 3, 22-25.
- Aitken, M.J., 1985. *Thermoluminescence Dating*, Academic Press, London.
- Antoine, P., 1991. Nouvelles données sur la stratigraphie du Pléistocène supérieur de la France septentrionale, d'après les sondages effectués sur le tracé du TGV Nord. *Publications du Centre d'Études et de Recherches Préhistoriques*, 3, 9-20.
- Antoine, P., 1994. The Somme Valley terrace system (Northern France); a model of river response to quaternary climatic variations since 800 000 BP. *Terra-Nova*, 6, 453-464.
- Antoine, P., 2012. Thermokarst processes and features from west-european loess series: new evidences for rapid climatic warning events during the Last Glacial. *Quaternary International*, 21, 279-280.
- Antoine, P., Lautridou, J.-P. Sommé, J., Auguste, P., Auffret, J.-P., Baize, S., Clet-Pellerin, M., Coutard, J.-P., Dewolf, Y., Dugué, O., Joly, F., Laignel, B., Laurent, M., Lavollé, M., Lebre, P., Lefebvre, D., Lécolle, F., Limondin-Lozouet, N., Munaut, A.-V., Ozouf, J.-C.,

- Quesnel, F., Rousseau, D.-D., 1998. Les formations quaternaires de la France du Nord-Ouest : limites et corrélations. *Quaternaire*, 9, 227-241.
- Antoine, P., Rousseau, D.-D., Lautridou, J.-P., Hatté, C., 1999. Last interglacial-glacial climatic cycle in loess-paleosol successions of north-western France. *Boreas*, 28, 551-563.
- Antoine, P., Rousseau, D.-D., Zöller, L., Lang, A., Munaut, A.V., Hatté, C., Fontugne, M., 2001. High resolution record of the last Interglacial-glacial cycle in the Nussloch loess-palaeosol sequences, Upper Rhine Area Germany. *Quaternary International*, 76-77, 211-229.
- Antoine, P., Auguste, P., Bahain, J.-J., Coudret, P., Depaepe, P., Fagnart, J.-P., Falguères, C., Fontugne M., Frechen., Hatté, C., Lamotte, A., Laurent, M., Limondin-Lozouet, N., Loch, J.-L., Mercier, N., Moigne, A.-M., Munaut, A.-V., Ponel, P., Rousseau, D.-D., 2003a. Paléoenvironnements pléistocènes et peuplements paléolithiques dans le bassin de la Somme (nord de la France). *Bulletin de la Société préhistorique française*, 100, 5-28.
- Antoine, P., Bahain, J.-J., Debenham, N., Frechen, M., Gauthier, A., Hatté, C., Limondin-Lozouet, N., Loch, J.-L., Raymond, P., Rousseau, D.-D., 2003b. Nouvelles données sur le Pléistocène du Nord du Bassin Parisien : les séquences loessiques de Villiers-Adam (Val d'Oise, France). *Quaternaire*, 14, 219-235.
- Antoine, P., Rousseau, D.-D., Moine, O., Kunesch, S., Hatté, C., Lang, A., Zöller, L., 2009. Evidence of rapid and cyclic eolian deposition during the Last Glacial in European loess series (Loess Events): the high-resolution records from Nussloch (Germany). *Quaternary Science Reviews* 28, 2955-2973.
- Antoine, P., Goval, E., Jamet, G., Coutard, S., Moine, O., Herisson, D., Auguste, P., Guérin, G., Lacroix, F., Schmidt, E., Robert, V., Debenham, N., Meszner, S., Bahain, J.-J. 2014a. Les séquences loessiques pléistocène supérieur d'Havrincourt (Pas-de-Calais, France) : stratigraphie, paléoenvironnement, géochronologie et occupations paléolithiques. *Quaternaire* 25 (4), 321-368.
- Antoine P., Loch J.-L., Limondin-Lozouet N., Auguste P., Bahain J.-J., Fagnart J.-P., Debenham N. & Ducrocq T. (2014b) – Quaternary geoarcheology and Prehistory: the model of the Somme valley (France) and the neighbouring regions. In Arnaud-Fassetta G. & Carcaud N. (Eds.) *French geoarchaeology in the 21st century*, CNRS éditions, Paris, 71-86.
- Antoine, P., Coutard, S., Guérin, G., Deschodt, L., Goval, E., Loch, J.-L., Paris, C., 2016. Upper Pleistocene loess-palaeosols records from Northern France in the European context:

- environmental background and dating of the Middle Palaeolithic. *Quaternary International* 411, 4-24.
- Bahain, J.-J., Falguères, C., Dolo, J.-M., Antoine, P., Auguste, P., Limondin-Lozouet, N., Loch, J.-L., Tuffreau, A., 2010. ESR/U-series dating of teeth recovered from well-stratigraphically age-controlled sequences from Northern France. *Quaternary Geochronology*, 5, 371-375.
- Bahain, J.-J., Falguères, C., Laurent, M., Dolo, J.-M., Shao, Q., Auguste, P., Tuffreau, A., 2015. ESR/U-series dating of faunal remains from the paleoanthropological site of Biache-Saint-Vaast (Pas-de-Calais, France). *Quaternary Geochronology*, 30, 541-546.
- Bahain, J.-J., Yokoyama, Y., Falguères, C., Sarcia, M.N., 1992. ESR dating of tooth enamel: a comparison with K-Ar dating. *Quaternary Science reviews*, 11, 245-250.
- Bøtter-Jensen, L., Bulur, E., Murray, A.S., Póolton, N.R.J., 2002. Enhancements in luminescence measurement techniques. *Radiation Protection Dosimetry*, 101, 119-124.
- Brennan, B.J., Rink, W.J., McGuirl, E.L., Schwarcz, H.P., Prestwich, W.V., 1997. Beta doses in tooth enamel by “One Group” theory and the Rosy ESR dating software. *Radiation Measurements*, 27, 307–314.
- Deschodt, L., Barbier, P., Djemali, N., Drwila, G., Feray, P., Teheux, E., 1998. Onnaing, Usine Toyota, Rapport des sondages archéologiques profonds. 06/98 Villeneuve d'Ascq. Institut National Archéologiques préventives, Rapport de sondage, Direction Régionale des Affaires Culturelles du Nord-Pas-de-Calais, Service Régional de l'Archéologie, 66 p.
- Duller, G.A.T., 2003. Distinguishing quartz and feldspar in single grain luminescence measurements. *Radiation Measurement*, 37, 161-165.
- Duval, M., Grün, R., 2016. Are published ESR dose assessments on fossil tooth enamel reliable? *Quaternary Geochronology*, 31, 19-27.
- Frechen, M., Schweitzer, U., Zander, A., 1996. Improvements in sample preparation for the fine grain technique. *Ancient TL*, 14, 15–17.
- Frechen, M., van Vliet-Lanoë, B., van den Haute, P., 2001. The Upper Pleistocene loess record at Harmignies/Belgium-high resolution terrestrial archive of climate forcing. *Paleogeography, Paleoclimatology, Paleoecology* 173, 175-195.
- Goval, E., Hérissou, D. (dir). (submitted). Les occupations moustériennes et gravettiennes d'Havrincourt (Pas-de-Calais, France). Approches taphonomiques, techno-économique, fonctionnelle et Spatiale des assemblages. ERAUL.
- Grün, R., Katzenberger-Apel, O., 1994. An alpha irradiator for ESR dating. *Ancient TL*, 12, 35–38.

- Grün, R., Schwarcz, H.P., Chadam, J.M., 1988. ESR dating of tooth enamel: coupled correction for U-uptake and U-series disequilibrium. *Nuclear Tracks and Radiation Measurements*, 14, 237-241.
- Guérin, G., 1982. Evaluation des débits annuels de dose utilisés pour la datation des coulées volcaniques. *PACT J*, 6, 179-187.
- Guérin, G., Mercier, N., Adamiec, G., 2011. Dose-rate conversion factors: update. *Ancient TL*, 29, 5–8.
- Guérin, G., Valladas, H., 2014. Cross-calibration between beta and gamma sources using quartz OSL: Consequences of the use of the SAR protocol in optical dating. *Radiation Measurements*, 68, 31-37.
- Haesaerts, P., 1985. Les loess du Pléistocène supérieur en Belgique. Comparaisons avec les séquences d'Europe centrale. *Bulletin de l'Association Française pour l'Etude du Quaternaire*, 22-23 (2-3), 105-115.
- Haesaerts, P., 2000. Pedosedimentary evolution of the last interglacial and early glacial sequence in the European loess belt from Belgium to central Russia. *Netherlands Journal of Geosciences*, 79, 313-324.
- Haesaerts, P., Borziac, I., Chekha, V.P., Chirica, V., Drozdov, N.I., Koulakovska, L., Orlova, L.A., van der Plicht, J., Damblon, F., 2010. Charcoal and wood remains for radiocarbon dating Upper Pleistocene loess sequences in Eastern Europe and Central Siberia. *Palaeogeography, Palaeoclimatology, Palaeoecology*, 29 (1-2), 106-127.
- Haesaerts, P., Borziak, I., Chirica, V., Damblon, F., Koulakovska, L., Van der Plicht, J., 2003. The East-Carpathian loess record: a reference for the Middle and Late Pleniglacial stratigraphy in Central Europe. *Quaternaire* 14 (3), 163-188.
- Haesaerts P., Damblon F., Gerasimenko N., Spagna P., Pirson S., 2016. The Late Pleistocene loess-palaeosol sequence of Middle Belgium. *Quaternary international*, 411 A, 25-43.
- Haesaerts, P., Juvigné, E., Kuyl, O., Mûcher, H., Roebroeks, W., 1981. Compte rendu de l'excursion du 13 Juin 1981, en Hesbaye et au Limbourg Néerlandais, consacrée à la chronostratigraphie des loess du Pléistocène supérieur. *Annales de la Société Géologique de Belgique* 104, 223-240.
- Haesaerts, P., Mestdagh, H., Bosquet, D., 1999. The sequence of Remicourt (Hesbaye-Belgium): new insights on the pedo and chronostratigraphy of the Rocourt Soil. *Geologica Belgica* 2 (3/43), 5-27.

- Haesaerts, P., Van Vliet-Lanoë, B., 1974. Compte-rendu de l'excursion du 25 mai 1974 consacrée à la stratigraphie des limons aux environs de Mons. *Annales de la Société Géologie et de Paléontologie* 978, 547-560
- Hérisson, D., Goval, E., 2013. Du Paléolithique inférieur au début du Paléolithique supérieur dans le Nord de la France : lumière sur les premières découvertes du Canal Seine-Nord Europe. *Notae Praehistoricae*, 33, 91-104.
- Hérisson, D., Coutard, S., Goval, E., Loch, J.-L., Antoine, P., Chantreau, Y., Debenham, N., 2016. A new key-site for the end of the Lower Palaeolithic and the onset of the Middle Palaeolithic at Etrécourt-Manancourt (Somme, France). *Quaternary International* 409 (B), 73-91.
- IAEA, 1987. Preparation of Gamma-ray Spectrometry Reference Materials RGU-1, RGTh-1 and RGK-1 Report - IAEA/RL/145, Vienna.
- JCGM 100, 2008. Evaluation of measurement data - Guide to the expression of uncertainty in measurement.
- Juvigné, E., Tallier, E., Haesaerts, P., Pirson, S., 2008. Un nouveau stratotype du Téphra de Rocourt dans la carrière de Romont (Eben/Bassenge, Belgique). *Quaternaire* 19 (2), 133-139.
- Lang, A., Lindauer, S., Kuhn, R., Wagner, G.A., 1996. Procedures used for optically and infrared stimulated luminescence dating of sediments in Heidelberg. *Ancient TL*, 14, 7-11.
- Lanos P., Philippe A. (2015) Event model: a robust Bayesian tool for chronological modeling. <hal-01241720> <https://hal.archives-ouvertes.fr/hal-01241720>
- Lanos P., Philippe A. (2017) Hierarchical Bayesian modeling for combining Dates in archaeological context. *Journal de la Société Française de Statistique*. To appear. <https://hal-insu.archives-ouvertes.fr/insu-01451452/document>
- Lautridou, J.-P., 1985. Le cycle périglaciaire pléistocène en Europe du Nord-Ouest et plus particulièrement en Normandie. Thèse Lettres. Univ. Caen, 908 p.
- Lautridou, J.P., Sommé, J., Heim, J., Puisségur, J.J., Rousseau, D.D., 1985. La stratigraphie des loess et formations fluviales d'Achenheim (Alsace) : nouvelles données bioclimatiques et corrélations avec les séquences pléistocènes de la France du Nord-Ouest. *Bulletin de l'Association Française pour l'Etude du Quaternaire* 22, 125-132.
- Locht, J.-L., Antoine, P., Auguste, P., Bahain, J.-J., Debenham, N., Falguères, C., Farkh, S., Tissoux, H., 2006. La séquence loessique pléistocène supérieur de Savy (Aisne France): stratigraphie, datations et occupations paléolithiques. *Quaternaire*, 17 (3), 269-275.

- 765 Loch, J.-L., Antoine, P., Auguste P., Caspar, P., Depaepe, P., Engelmann, A., Frechen, M.,
 766 Michel, V., Munaut, A.-V., Révillon, S., Swinnen, C., 2002. Le site de Bettencourt-Saint-
 767 Ouen (Somme), cinq occupations du Paléolithique moyen au début de la dernière
 768 glaciation. Paris, éd. de la Maison des sciences de l'Homme. Documents d'Archéologie
 769 Française, 90, 168 p.
- 770 Loch, J.-L., Antoine, P., Bahain, J.-J., Dwirila, G., Raymond, P., Limondin-Lozouet, N.,
 771 Gauthier, A., Debenham, N., Frechen, M., Rousseau, D.-D., Hatté, C., Haesaerts, P.,
 772 Metsdag, H., 2003. Le gisement paléolithique moyen et les séquences pléistocènes de
 773 Villiers-Adam (Val d'Oise, France) : Chronostratigraphie, Environnement et Implantations
 774 humaines. Gallia Préhistoire, 45, 3-104.
- 775 Loch, J.L., Swinnen, C., Antoine, P., Révillon, S., Depaepe, P., 2002. Le Gisement
 776 paléolithique moyen de Bettencourt-Saint-Ouen (Somme). L'Acheuléen dans la vallée de la
 777 Somme : données récentes. Publications du Centre d'Etudes et de Recherches
 778 Préhistoriques 6, 199-237.
- 779 Loch J.-L., Hérison D., Goval E., Cliquet D., Huet B., Coutard S., Antoine P., Feray P.,
 780 2016. Timescales, space and culture during the Middle Palaeolithic in northwestern France.
 781 Quaternary International, 411 A, 129-148.
- 782 Marcy, T., Sellier, N., Devred, V., Dubois, S., 2009. Bourlon, Havrincourt, Graincourt-lès-
 783 Havrincourt, Sains-lès-Marquions (Pas-de-Calais). Rapport de diagnostic de la ZD7, Canal
 784 Seine-Nord Europe, Institut National de Recherches Archéologiques Préventives, Croix-
 785 Molineaux, 116 p.
- 786 Meijs, E.P.M., 2002. Loess stratigraphy in Dutch and Belgian Limburg. Eiszeitalter und
 787 Gegenwart 51, 11-130.
- 788 Meijs, E.P.M., 2011. The Veldwezelt site (province of Limburg, Belgium), environmental and
 789 stratigraphical interpretations. In: Jagt, J.W.M., Jagt-Yazykova, E.A., Schins, W.J.H. (Eds.),
 790 A Tribute to the Late Felder Brothers-Pioneers of Limburg Geology and Archaeology,
 791 Netherland Journal of Geosciences, 90 (2-3), 73-94.
- 792 Mercier, N., Falguères, C., 2007. Field gamma dose-rate measurement with a NaI(Tl)
 793 detector: re-evaluation of the "threshold" technique. Ancient TL 25, 1-4.
- 794 Moine, O., Antoine, P., Deschodt, L., Sellier, N., 2011. Enregistrements malacologiques à
 795 haute résolution dans les loess et les gleys de toundra du pléniglaciaire weichselien
 796 supérieur : premiers exemples du nord de la France. Quaternaire, 22 (4), 307-325.

- Moine, O., Rousseau, D.-D., Antoine, P., 2008. Abrupt malacological and lithological changes along the Upper Weichselian loess sequence of Nussloch (Rhine Valley, Germany). *Quaternary Research* 70, 91-104.
- Murray, A.S., Olley, J.M., 2002. Precision and accuracy in the optically stimulated luminescence dating of sedimentary quartz: a status review. *Geochronometria*, 21, 1-16.
- Murray, A.S., Wintle, A.G. 2000: Luminescence dating of quartz using an improved single aliquot regenerative-dose protocol. *Radiation Measurements*, 32, 57-73.
- Murray, A.S., Wintle, A.G., 2003. The single aliquot regenerative dose protocol: potential for improvements in reliability. *Radiation Measurements* 37, 377–381.
- Philippe A., Vibet M.-A. (2017) Analysis of Archaeological Phases using the CRAN Package ArchaeoPhases.. <https://halshs.archives-ouvertes.fr/FMPL/hal-01347895v3>
- Prescott, J.R., Hutton, J.T., 1994. Cosmic ray contribution to dose rates for luminescence and ESR dating: large depths and long-term time variations. *Radiation Measurements*, 23, 497-500.
- Prescott, J.R., Stephan, L.G., 1982. The contribution of cosmic radiation to the environmental dose for thermoluminescence dating. *PACT*, 6, 17-25.
- Rees-Jones, J., Tite, M.S., 1997. Optical dating results for British archaeological sediments. *Archaeometry* 39, 177-187.
- Rousseau, D.-D., Antoine, P., Hatté, C., Lang, A., Zöller, L., Fontugne, M., Ben Othman, D., Luck, J.M., Moine, O., Labonne, M., Bentaleb, I., Jolly, D., 2002. Abrupt millennial climatic changes from Nussloch (Rhine Valley, Germany) eolian (loess) records during the Last Glaciation. *Quaternary Science Reviews* 21, 1577-1582.
- Rousseau, D.-D., Sima, A., Antoine, P., Hatté, C., Lang, A., Zöller, L., 2007. Link between European and North-Atlantic abrupt climate changes over the last glaciation. *Geophysical Research Letters* 34, 22.
- Sellier, N., 2005. Bapaume, le Petit Moulin, rapport de diagnostic, Inrap Nord-Picardie, 15 p.
- Shao, Q., Bahain, J.-J., Dolo, J.-M., Falguères, C., 2014. Monte Carlo approach to calculate US-ESR ages and their uncertainties. *Quaternary Geochronology*, 22, 99-106.
- Shao, Q., Bahain, J.-J., Falguères, C., Dolo, J.-M., Garcia, T., 2012. A new U-uptake model for combined ESR/U-series dating of tooth enamel. *Quaternary Geochronology*, 10, 406-411.

- Shao, Q., Bahain, J.-J., Wang, W., Jin, C., Wang, Y., Voinchet, P., Lin, M., 2016. Combined ESR and U-series dating of early Pleistocene Gigantopithecus faunas at Mohui and Sanhe Caves, Guangxi, southern China. *Quaternary Geochronology*, 30, 524-528.
- Sommé, J., 1975. Les plaines du Nord de la France et leur bordure : étude géomorphologique. Thèse de Doctorat d'État, Université Paris 1 Panthéon-Sorbonne, Paris, 3 vol., 790 p.
- Valladas, H., Valladas, G., 1982. Effet de l'irradiation alpha sur les grains de quartz. *PACT J*, 6, 171-178.
- Vallin, L., Masson, B., 2003. Le gisement moustérien d'Hermies. Le Tio Marché. Rapport de fouille programmée, campagne 2002, SRA Nord-Pas-de-Calais, 34 p.
- Vandenbergh, D., 2004. Investigation of the Optically Stimulated Luminescence Dating Method for Application to Young Geological Sediments. PhD thesis. Ghent University, 358 pp.
- Wang, X.L., Wintle, A.G., Du, J.H., Kang, S.G., Lu, Y.C., 2011. Recovering laboratory doses using fine-grained quartz from Chinese loess. *Radiation Measurements*, 46, 1073-1081.
- Vibet M.-A., Philippe A., Lanos P., Dufresne P. (2016) ChronoModel V1.5 User's manual. www.chronomodel.fr.
- Wintle, A.G., Murray, A.S., 2006. A review of quartz optically stimulated luminescence characteristics and their relevance in single-aliquot regeneration dating protocols. *Radiation Measurements*, 41, 369–391.

Figure caption

Figure 1. Location of the Havrincourt site in the European Loess belt (according to Antoine et al., 2003a, modified). 1: Loess (>4m) 2: Loess (<4m) 3: Sandy loess

Figure 2. Location and view of the Havrincourt excavation area and location of the sampled profiles (after Antoine et al., 2014, modified).

Figure 3. Stratigraphy and litho-chronological interpretation of the Havrincourt sequence (after Antoine et al., 2014, modified).

Figure 4. Lithic industry of Havrincourt. 1-4: Middle Palaeolithic pieces: 1 & 2 - Hav.1-N3 – Large Levallois flakes; 3. Hav.2-N0 – Levallois point; 4. Hav.2- N1 - Levallois core ; 5. Upper Palaeolithic Hav.2-N2 – Lithic refitting showing the blade production (drawns by Eve Boitard-Bidaut, Inrap)

Figure 5. Location of the OSL samples on the Havrincourt profiles. Description of the units is in Fig. 3.

Figure 6. OSL curves of natural (squares) and regenerated quartz (90 Gy, solid line). Dose–response curve of HAV2 P5-4 is fitted with a linear plus saturating exponential function. Recycling ratios are indistinguishable from unity and the growth curve pass very close to the origin. Preheat temperature for this example is 260 °C.

Figure 7. Preheat plateau test (plain square), recycling ratio of HAV2 P5-1 (open diamond) and additive recovery test (open circles), representative of the quartz behaviour from Havrincourt loesses. Additive recovery test was achieved by adding 85.1 Gy to the natural sample.

Figure 8. Modeling done with ChronoModel.

Black outlined nodes represent an event. The name written into the node is the name of the date associated to this event and the shape corresponds to the used dating method. An arrow between two events symbolizes a temporal relationship, the arrow heading from the oldest event to the youngest one. At Havrincourt, we have considered 25 events, 17 OSL dates, 8 associated to TL/ESR/14C dates, and temporal relationships.

Grey outlined node symbolizes a group of events. An arrow between two groups symbolises a temporal relationship, the arrow heading from the oldest group to the youngest one.

Figure 9. Densities of the minimum and the maximum of each group of dates (here referring to an unit). Results are represented in years before 2016 AD

Figure 10. Summary pedo-lithostratigraphic sequence for northern France,

chronostratigraphy, dating and correlation with Havincourt and Remicourt (Belgium) sites

Northern France synthetic record units - 1: surface soil (a: Ap. horizon; b: Bt horizon; c: banded Bt horizon); 2: homogeneous calcareous loess; 3: greyish and lightly humic tundra gley with tongued horizon (Nagelbeek Hz.); 4: carbonated laminated loess with cryo-dessication micro-cracks; 5: cryoturbated tundra gley doublet with intermediary loess (5b); 6: homogeneous calcareous loess; 7: cryoturbated tundra gley Hz. & large ice-wedges network (F-4); 8: arctic brown soil / or soil complex; 9: sandy silts or calcareous loess; 10: greyish tundra gley horizon; 11: humic horizon / arctic meadow type soil; 12: brown Boreal soil complex; 13: heterogeneous bedded slope deposits and sandy silts (thermokarst gully infilling); 14: homogeneous calcareous loess; 15: thin tundra gley doublet (15a-c) including a calcareous loess unit (15b); 16: homogeneous brownish non calcareous colluvial silts / incipient soil (arctic meadow Hz.); 17: laminated colluvial deposits reworking soil lenses and soil nodules with frost cracks; 18: brownish-greyish non-calcareous loess; 19 to 22: steppe-like soils with interstratified unit of local, non-carbonated loess (MS / 20); 23b: grey forest soil on colluviums; 23a: bleached horizon; 24b: clayey colluviums/grey forest soil (Bettencourt Soil); 24a: bleached horizon; 25b: Bt horizon of brown leached soil (Rocourt/Elbeuf 1); 25a: bleached horizon; 26: Saalian calcareous loess.

Unit abbreviations - France (According to Antoine et al, 2016) - ELB1/SDS: Elbeuf 1 / Sourdon soil horizons (Eemian); BSO: Bettencourt-Saint-Ouen soil horizon; SS1 to SS3b: Saint-Sauflieu soil horizons; HBS: Havrincourt brown silts - *Belgium* (According to Haesaerts et al, in press) - HS: Harmignies soil horizon (Eemian); VSG (A&B): Villers-Saint-Ghislain A and B soil horizons; MPS: Malplaquet soil horizon; SV-HB4: Les Vaux Soil horizon

Freeze structures - A: large ice-wedge casts; B: small wedges with soil infilling; C: frost-creep, solifluction, gelifluction; D: ice-melt channels (thermokarst); E: Large incision features (thermokarst erosion gullies)

Site name abbreviations - FaV: Fresnoy au Val; SD: Sourdon; BG: Beugnâtre; Herm.: Hermies; Havr.: Havrincourt; VA: Villiers-Adam; BsO: Bettencourt-Saint-Ouen; SSL: Saint-Sauflieu.

Archaeological level with TL dating from heated flints (numbers, Locht et al, 2016) and ESR/U-series on teeth and bones (letters, Locht et al, 2006)- 1) Villiers-Adam: 110 ± 11 ka; 2) Fresnoy-au-Val: 106.8 ± 7.5 ka; 3) Saint-Hilaire-sur-Helpe: 98.9 ± 9.3 ka; 4) Mauquenchy Low.: 83 ± 7.6 ka, 5); Mauquenchy Upp.: 77.0 ± 7.2 ka; 6) Beauvais: 55.6 ± 4 ka; A) Savy low.: 51 ± 3 ka; B) Savy upp.: 30 ± 2 ka.

Table caption

Table 1. Details of the SAR protocol used in this study (modified from Murray and Wintle 2000). TPH is the preheat temperature determined for each sample using a preheat plateau test and dose recovery tests. Most frequent value for TPH is 260 °C.

(*) The cycle is repeated twice with an IR-stimulation at 50 °C for 44 s between the steps 2-3.

Table 2. SAR measurements results.

Table 3. Havrincourt OSL samples. U, Th and K concentrations measured by gamma spectroscopy and parameters used for annual dose rate calculation (Sample depth from the surface; ratio of the water weight at saturation to dry sample weight; alpha efficiency determined using a ^{241}Am calibrated source).

Table 4. ESR/U-series parameters used for the Havrincourt horse teeth.

Table 5. C14 dates obtained on fossil bones from Havrincourt (calibrations according to Reimer et al. (2013), IntCal13)

Table 6. Age results. Annual dose rates are calculated using table 3 data and most recent revised conversion factors (Guérin et al. 2011). Corrections due to moisture are calculated by applying a uniform factor, 0.8 ± 0.12 , to the water saturation level. Uncertainties on equivalent dose include a 1.2% error on the beta source calibration.

Table 7. ESR/U-series age results for the Havrincourt horse teeth. (a) A k-value of 0.13 ± 0.02 was used according to Grün and Katzenberger-Appel (1994); (b) Cosmic dose was estimated from the Prescott and Hutton's data (1994); (c) Uncertainties on the ESR/U-series ages (model US, Grün et al. 1988 or model AU, Shao et al. 2012) were calculated using Monte-Carlo approach (Shao et al., 2014).

Supplementary material

Figure S1. *Time range interval* for the units succession of Havrincourt. Results are represented in years before 2016 AD. Segments to time range of the phase associated to a level confidence of 95%.

Table S1. Activity (Bq/kg) of main natural radionuclides of U and Th decay chains of the Havrincourt OSL sediment samples measured by gamma spectroscopy ($^{234}\text{Th1}$ and $^{234}\text{Th2}$ correspond to 63.3keV and 92.3 keV gamma emissions respectively).

Table S2. Time range endpoints for Havrincourt units (at level 95%). Results are represented in years before 2016 AD.

Step	OSL measurements	
1	Given dose: 0 (Nat), R1, R2, R3, R4, 0, R1, R1*	
2	Preheat at T_{PH} for 10 s	
3	OSL at 125 °C for 44 s	Lx
4	Test dose 10 Gy	
5	Cutheat 180 °C for 1 s	
6	OSL at 125 °C for 44 s	Tx
-	Back to step 1	

Sample	m (g)	^{210}Pb	$^{234}\text{Th1}$	$^{234}\text{Th2}$	^{226}Ra	Pb/Ra	Ra/U	^{228}Ra	^{228}Th	$^{228}\text{Ra}/^{226}\text{Ra}$	$^{228}\text{Th}/^{226}\text{Ra}$	U (ppm)	Th (ppm)
HAV1-P1-1	2.44	42.1 ± 5.1	36 ± 5	56.0 ± 4.0	41.7 ± 1.0	1.0	1.2	44.6 ± 2.2	43 ± 1	1.07 ± 0.06	0.97 ± 0.05	2.90 ± 0.40	10.59 ± 0.27
HAV1-P1-2	2.83	43.2 ± 2.8	42 ± 3	54.0 ± 2.0	42.7 ± 0.6	1.0	1.0	45.3 ± 1.2	46 ± 1	1.06 ± 0.03	1.02 ± 0.03	3.39 ± 0.24	11.35 ± 0.15
HAV1-P1-3	3.02	44.2 ± 5.0	51 ± 5	54.0 ± 3.0	41.4 ± 1.0	1.1	0.8	50.2 ± 2.1	48 ± 1	1.21 ± 0.06	0.95 ± 0.05	4.11 ± 0.40	11.77 ± 0.27
HAV1-P1-4	2.84	40.4 ± 5.1	41 ± 5	49.9 ± 3.4	40.8 ± 0.9	1.0	1.0	47.4 ± 1.9	52 ± 1	1.16 ± 0.05	1.11 ± 0.05	3.32 ± 0.40	12.87 ± 0.27
HAV1-P1-5	3.17	38.2 ± 4.7	41 ± 4	54.0 ± 3.0	42.1 ± 0.9	0.9	1.0	49.5 ± 2.0	49 ± 1	1.18 ± 0.05	1.00 ± 0.05	3.31 ± 0.32	12.14 ± 0.25
HAV1-P1-6	2.76	52.9 ± 5.2	48 ± 5	53.0 ± 3.0	42.3 ± 1.0	1.3	0.9	45.7 ± 2.1	48 ± 1	1.08 ± 0.06	1.04 ± 0.05	3.87 ± 0.40	11.67 ± 0.27
HAV1-P1-7	2.49	48.9 ± 3.0	50 ± 3	64.0 ± 2.0	43.9 ± 0.6	1.1	0.9	54.7 ± 1.4	54 ± 1	1.25 ± 0.04	0.98 ± 0.03	-	-
HAV1-P1-7	2.49	47.4 ± 3.8	54 ± 4	50.0 ± 2.0	41.3 ± 0.7	1.1	0.8	52.2 ± 1.3	54 ± 1	1.43 ± 0.04	1.03 ± 0.03	-	-
HAV1-P1-7	-	48.3 ± 2.4	51 ± 2	57.0 ± 1.4	42.8 ± 0.5	-	-	53.36 ± 1.0	54 ± 1	1.32 ± 0.03	1.00 ± 0.02	4.15 ± 0.19	13.19 ± 0.13
HAV1-P1-8	2.79	41.4 ± 6.0	48 ± 6	46.0 ± 4.0	40.1 ± 1.2	1.0	0.8	48.3 ± 2.5	50 ± 1	1.20 ± 0.07	1.03 ± 0.06	-	-
HAV1-P1-8	2.79	39.1 ± 3.9	37 ± 3	47.0 ± 3.0	38.1 ± 0.7	1.0	1.0	36.9 ± 1.3	41 ± 1	0.97 ± 0.04	1.12 ± 0.04	-	-
HAV1-P1-8	-	39.8 ± 3.3	39 ± 3	46.6 ± 2.4	38.6 ± 0.6	1.0	1.0	39.33 ± 1.2	44 ± 1	1.02 ± 0.03	1.08 ± 0.04	3.16 ± 0.22	10.70 ± 0.17
HAV1-P1-9	3.09	39.8 ± 2.8	41 ± 3	57.0 ± 2.0	39.6 ± 0.5	1.0	1.0	51.5 ± 1.2	49 ± 1	1.30 ± 0.03	0.96 ± 0.03	3.31 ± 0.24	12.11 ± 0.15
HAV1-P3-10	4.13	35.1 ± 3.5	33 ± 3	42.5 ± 2.3	32.8 ± 0.6	1.1	1.0	36.1 ± 1.2	35 ± 1	1.10 ± 0.04	0.98 ± 0.04	2.68 ± 0.27	8.65 ± 0.15
HAV2-P5-1	3.48	41.3 ± 3.8	42 ± 4	46.8 ± 2.6	34.8 ± 0.6	1.2	0.8	40.9 ± 1.1	41 ± 1	1.18 ± 0.04	1.01 ± 0.03	3.41 ± 0.31	10.15 ± 0.17
HAV2-P5-2	3.87	37.1 ± 3.4	38 ± 3	42.3 ± 2.4	38.3 ± 0.6	1.0	1.0	35.6 ± 1.2	36 ± 1	0.93 ± 0.03	1.01 ± 0.04	3.06 ± 0.27	8.85 ± 0.15
HAV2-P5-4	2.83	54.6 ± 4.9	46 ± 5	58.0 ± 3.0	43.1 ± 1.0	1.3	0.9	51.5 ± 2.2	49 ± 1	1.19 ± 0.06	0.94 ± 0.05	3.71 ± 0.40	11.94 ± 0.27
HAV2-P5-5	3.87	39.1 ± 2.0	41 ± 2	49.1 ± 1.4	38.4 ± 0.3	1.0	0.9	46.7 ± 0.6	47 ± 1	1.22 ± 0.02	1.00 ± 0.02	3.28 ± 0.17	11.45 ± 0.10
HAV2-P5-8	2.81	44.8 ± 4.9	41 ± 5	48.0 ± 3.0	33.3 ± 0.9	1.3	0.8	44.8 ± 2.0	43 ± 1	1.35 ± 0.07	0.96 ± 0.05	3.31 ± 0.40	10.59 ± 0.25
HAV2-P6-1	3.97	45.2 ± 3.8	42 ± 4	52.4 ± 2.5	38.6 ± 0.6	1.2	0.9	44.9 ± 1.2	47 ± 1	1.16 ± 0.04	1.04 ± 0.03	3.38 ± 0.31	11.45 ± 0.17
HAV2-P6-2	3.68	33.9 ± 3.7	40 ± 4	48.4 ± 2.5	40.6 ± 0.6	0.8	1.0	48.0 ± 1.2	47 ± 1	1.18 ± 0.03	0.97 ± 0.03	3.20 ± 0.30	11.47 ± 0.17

Supplementary table 1. Activity (Bq/kg) of main natural radionuclides of U and Th decay chains of the Havrincourt OSL sediment samples measured by gamma spectroscopy.

Sample	Sector	Profile	Unit	Preheat temperature (°C)	Recycling ratio	IR depletion ratio	Recuperation ratio (%)	Recovery test
HAV1-P1-1	HAV1	P1	4	260	1.00 ± 0.01	0.99 ± 0.01	1.1	0.98 ± 0.01
HAV1-P1-2	HAV1	P1	5a	260	1.00 ± 0.01	1.01 ± 0.01	1.2	1.01 ± 0.01
HAV1-P1-3	HAV1	P1	5a	260	1.00 ± 0.01	0.98 ± 0.01	1.0	1.00 ± 0.01
HAV1-P1-4	HAV1	P1	6b	260	0.99 ± 0.01	0.98 ± 0.01	0.9	0.98 ± 0.01
HAV1-P1-5	HAV1	P1	7	260	0.98 ± 0.01	1.00 ± 0.01	1.1	1.00 ± 0.01
HAV1-P1-6	HAV1	P1	7	260	0.98 ± 0.01	1.00 ± 0.01	1.0	0.98 ± 0.02
HAV1-P1-7	HAV1	P1	8	260	0.98 ± 0.01	0.99 ± 0.01	1.1	0.98 ± 0.01
HAV1-P1-8	HAV1	P1	8	260	0.98 ± 0.01	1.01 ± 0.01	1.0	0.96 ± 0.01
HAV1-P1-9	HAV1	P1	10	260	0.98 ± 0.01	1.00 ± 0.01	0.9	0.97 ± 0.01
HAV1 P3-10	HAV1	P3	4	270	1.01 ± 0.01	0.98 ± 0.01	1.9	1.02 ± 0.01
HAV2-P5-1	HAV2	P5	2	280	0.99 ± 0.01	1.00 ± 0.01	2.0	0.98 ± 0.01
HAV2 P5-2	HAV2	P5	4	270	0.99 ± 0.01	1.00 ± 0.01	1.2	1.01 ± 0.01
HAV2-P5-4	HAV2	P5	6a	260	1.01 ± 0.01	1.00 ± 0.01	1.5	0.99 ± 0.01
HAV2 P5-5	HAV2	P5	7	270	1.01 ± 0.01	1.00 ± 0.01	1.3	0.96 ± 0.01
HAV2-P5-8	HAV2	P5	8	260	0.98 ± 0.01	1.00 ± 0.00	1.0	0.98 ± 0.01
HAV2 P6-1	HAV2	P6	12	260	0.99 ± 0.01	0.99 ± 0.01	1.2	0.98 ± 0.01
HAV2 P6-2	HAV2	P6	12	250	1.00 ± 0.01	0.99 ± 0.01	1.3	0.96 ± 0.02

Table 2. SAR measurements results. Uncertainties on equivalent dose include a 1.2% error on the beta source calibration.

Havrincourt stratigraphical units	Time Range lower bound	Time Range upper bound
US2	29 330	16 669
US4	31 026	23 450
US5	31 536	28 304
<i>Hav2-N2 archaeological level</i>	<i>37 014</i>	<i>30 423</i>
US6	43 846	30 494
<i>US7 (rodents bones)</i>	46 668	42 406
US7	59 051	45 070
US8	66 082	50 511
US10	70 348	57 290
<i>Hav2-N1 archaeological level</i>	<i>74 026</i>	<i>61 422</i>
US12	103 720	61 070

Table S2. Time range endpoints for Havrincourt units (at level 95%). Results are represented in years before 2016 AD.

Sample	Sector	Profile	Unit	Depth (cm)	U (ppm)	Th (ppm)	K (%)	Water (%)	Alpha efficiency factor (a-value)
HAV1-P1-1	HAV1	P1	4	270	2.89 ± 0.40	10.62 ± 0.27	1.27 ± 0.05	35.0 ± 3.5	0.0446 ± 0.0023
HAV1-P1-2	HAV1	P1	5a	300	3.38 ± 0.24	11.39 ± 0.15	1.29 ± 0.02	43.9 ± 4.4	0.0413 ± 0.0035
HAV1-P1-3	HAV1	P1	5a	320	4.10 ± 0.40	11.81 ± 0.27	1.35 ± 0.04	42.2 ± 4.2	0.0443 ± 0.0027
HAV1-P1-4	HAV1	P1	6b	350	3.31 ± 0.40	12.92 ± 0.27	1.37 ± 0.05	39.3 ± 3.9	0.0405 ± 0.0021
HAV1-P1-5	HAV1	P1	7	370	3.30 ± 0.32	12.18 ± 0.25	1.34 ± 0.04	39.4 ± 3.9	0.0407 ± 0.0021
HAV1-P1-6	HAV1	P1	7	415	3.86 ± 0.40	11.71 ± 0.27	1.42 ± 0.05	38.4 ± 3.8	0.0414 ± 0.0020
HAV1-P1-7	HAV1	P1	8	450	4.14 ± 0.19	13.23 ± 0.13	1.65 ± 0.02	42.9 ± 4.3	0.0417 ± 0.0023
HAV1-P1-8	HAV1	P1	8	470	3.15 ± 0.22	10.73 ± 0.17	1.28 ± 0.03	38.2 ± 3.8	0.0394 ± 0.0019
HAV1-P1-9	HAV1	P1	10	500	3.30 ± 0.24	12.15 ± 0.15	1.52 ± 0.03	41.8 ± 4.2	0.0405 ± 0.0020
HAV1 P3-10	HAV1	P3	4	270	2.67 ± 0.27	8.68 ± 0.15	1.22 ± 0.01	36.1 ± 3.6	0.0453 ± 0.0024
HAV2-P5-1	HAV2	P5	2	170	3.40 ± 0.31	10.18 ± 0.17	1.41 ± 0.03	43.1 ± 4.3	0.0437 ± 0.0023
HAV2 P5-2	HAV2	P5	4	280	3.05 ± 0.27	8.87 ± 0.15	1.20 ± 0.03	39.0 ± 3.9	0.0424 ± 0.0022
HAV2-P5-4	HAV2	P5	6a	345	3.70 ± 0.40	11.98 ± 0.27	1.37 ± 0.04	43.8 ± 4.4	0.0416 ± 0.0025
HAV2 P5-5	HAV2	P5	7	410	3.27 ± 0.17	11.49 ± 0.10	1.37 ± 0.03	48.4 ± 4.8	0.0422 ± 0.0021
HAV2-P5-8	HAV2	P5	8	495	3.30 ± 0.40	10.62 ± 0.25	1.41 ± 0.04	38.5 ± 3.9	0.0401 ± 0.0019
HAV2 P6-1	HAV2	P6	12	530	3.37 ± 0.31	11.49 ± 0.17	1.58 ± 0.03	50.1 ± 5.0	0.0391 ± 0.0018
HAV2 P6-2	HAV2	P6	12	550	3.19 ± 0.30	11.51 ± 0.17	1.67 ± 0.03	49.5 ± 5.0	0.0406 ± 0.0021

Table 3. Havrincourt OSL samples. U, Th and K concentrations measured by gamma spectroscopy and parameters used for annual dose rate calculation (Sample depth from the surface; ratio of the water weight at saturation to dry sample weight; alpha efficiency determined using a ^{241}Am calibrated source).

Sample	Unit	Archaeological Level	Tissue	Initial thickness (μm)	Removed thickness dentine side (μm)	Removed thickness sediment side (μm)	$^{234}\text{U}/^{238}\text{U}$	$^{230}\text{Th}/^{234}\text{U}$	$^{222}\text{Rn}/^{230}\text{Th}$	U (ppm)	Th (ppm)	K (%)
HAV1201	US6a	HAV2-N2	dentine enamel	1259 ± 157	147 ± 18	92 ± 12	1.130 ± 0.008 1.170 ± 0.008	0.097 ± 0.001 0.282 ± 0.001	0.52 1.00	4.10 ± 0.40	11.81 ± 0.27	1.35 ± 0.04
HAV1202	US12	HAV2-N1	dentine enamel	1527 ± 191	230 ± 29	166 ± 21	1.430 ± 0.007 1.449 ± 0.04	0.443 ± 0.004 0.355 ± 0.002	0.27 1.00	3.30 ± 0.40	10.62 ± 0.25	1.41 ± 0.04

Table 4. ESR/U-series parameters used for the Havrincourt horse teeth.

Site number	Lab number	Material	Unit	Archaeological Level	$^{13}\text{C}/^{12}\text{C}$ (‰)	^{14}C BP age (a)	^{14}C cal BP range (2 σ) (a)
HAV F 1384GL	Oxford P-30581	Bone	6a	Hav2-N2	Failed due to low yield		
HAV2 F1384GL	Beta - 307416	Bone	6a	Hav2-N2	-21.4	27020 \pm 140	31264-31851
HAV F 1419A	Oxford P-30580	Bone	6a	Hav2-N2	Failed due to low yield		
HAV2 F1801A L19	Beta - 332604	Bone	6a	Hav2-N2	-20.9	28100 \pm 180	31414-32572
HAV F 2034A	Oxford P-30582	Bone	6a	Hav2-N2	Failed due to low yield		
HAV2 F840 H	Beta -328569	Marmot bones	7	--	-20.5	42090 \pm 380	44740-46154
HAV2 F941G1	Beta -328570	Ground squirrel bones	7	--	-20.8	40100 \pm 370	43058-44462

Table 5. C14 dates obtained on fossil bones from Havrincourt (calibrations according to Reimer et al. (2013), IntCal13)

Sample	Sector	Profile	Unit	Equivalent dose (Gy)	Annual dose rate (mGy/year)					Age (ka)
					alpha	beta	gamma	cosmic	total	
HAV1-P1-1	HAV1	P1	4	80.9 ± 1.5	0.50 ± 0.05	1.28 ± 0.08	0.87 ± 0.05	0.15 ± 0.02	2.80 ± 0.18	28.9 ± 1.9
HAV1-P1-2	HAV1	P1	5a	87.7 ± 1.6	0.48 ± 0.05	1.28 ± 0.08	0.89 ± 0.05	0.14 ± 0.01	2.79 ± 0.17	31.4 ± 2.0
HAV1-P1-3	HAV1	P1	5a	97.4 ± 1.8	0.59 ± 0.06	1.41 ± 0.09	0.98 ± 0.06	0.14 ± 0.01	3.12 ± 0.20	31.2 ± 2.1
HAV1-P1-4	HAV1	P1	6b	126.6 ± 2.2	0.52 ± 0.05	1.39 ± 0.09	0.98 ± 0.06	0.13 ± 0.01	3.01 ± 0.19	42.1 ± 2.8
HAV1-P1-5	HAV1	P1	7	150.1 ± 2.7	0.50 ± 0.05	1.35 ± 0.08	0.95 ± 0.05	0.13 ± 0.01	2.93 ± 0.17	51.2 ± 3.1
HAV1-P1-6	HAV1	P1	7	178.4 ± 3.2	0.55 ± 0.05	1.46 ± 0.09	1.00 ± 0.06	0.12 ± 0.01	3.13 ± 0.19	57.0 ± 3.6
HAV1-P1-7	HAV1	P1	8	165.0 ± 2.9	0.59 ± 0.05	1.60 ± 0.09	1.08 ± 0.06	0.12 ± 0.01	3.39 ± 0.19	48.7 ± 2.9
HAV1-P1-8	HAV1	P1	8	177.5 ± 3.2	0.45 ± 0.04	1.29 ± 0.07	0.88 ± 0.05	0.11 ± 0.01	2.73 ± 0.15	65.0 ± 3.8
HAV1-P1-9	HAV1	P1	10	202.1 ± 2.4	0.49 ± 0.04	1.43 ± 0.08	0.96 ± 0.05	0.11 ± 0.01	2.99 ± 0.17	67.6 ± 3.9
HAV1 P3-10	HAV1	P3	4	84.0 ± 1.8	0.44 ± 0.04	1.18 ± 0.06	0.77 ± 0.04	0.15 ± 0.02	2.53 ± 0.14	33.2 ± 2.0
HAV2-P5-1	HAV2	P5	2	81.3 ± 2.0	0.49 ± 0.05	1.33 ± 0.08	0.87 ± 0.05	0.17 ± 0.02	2.86 ± 0.17	28.4 ± 1.8
HAV2 P5-2	HAV2	P5	4	84.1 ± 1.8	0.44 ± 0.04	1.19 ± 0.07	0.78 ± 0.04	0.14 ± 0.01	2.55 ± 0.15	33.0 ± 2.1
HAV2-P5-4	HAV2	P5	6a	103.6 ± 2.0	0.52 ± 0.05	1.37 ± 0.09	0.95 ± 0.06	0.13 ± 0.01	2.97 ± 0.19	34.9 ± 2.3
HAV2 P5-5	HAV2	P5	7	140.5 ± 3.1	0.47 ± 0.04	1.27 ± 0.08	0.87 ± 0.05	0.12 ± 0.01	2.73 ± 0.16	51.5 ± 3.2
HAV2-P5-8	HAV2	P5	8	176.4 ± 3.2	0.47 ± 0.05	1.37 ± 0.08	0.91 ± 0.06	0.11 ± 0.01	2.86 ± 0.18	61.7 ± 4.0
HAV2 P6-1	HAV2	P6	12	209.3 ± 4.7	0.44 ± 0.04	1.38 ± 0.09	0.91 ± 0.06	0.11 ± 0.01	2.83 ± 0.18	73.9 ± 5.0
HAV2 P6-2	HAV2	P6	12	262.7 ± 6.9	0.44 ± 0.04	1.42 ± 0.09	0.91 ± 0.06	0.10 ± 0.01	2.87 ± 0.18	91.5 ± 6.2

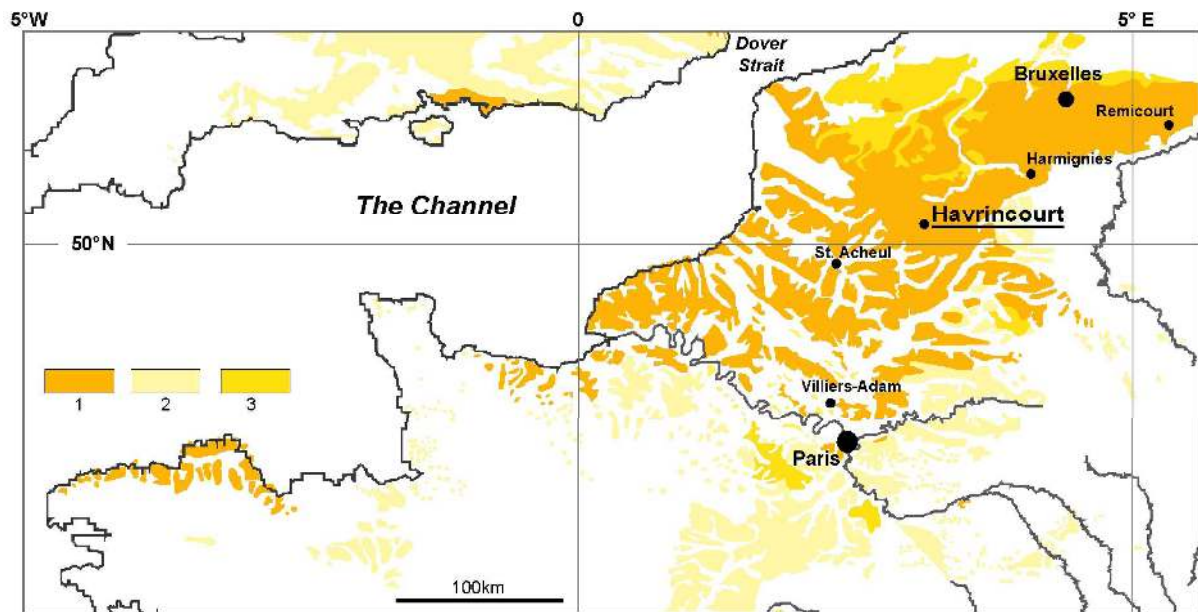
Table 6. Age results. Annual dose rates are calculated using table 3 data and most recent revised conversion factors (Guérin et al. 2011). Corrections due to moisture are calculated by applying a uniform factor, 0.8 ± 0.12 , to the water saturation level.

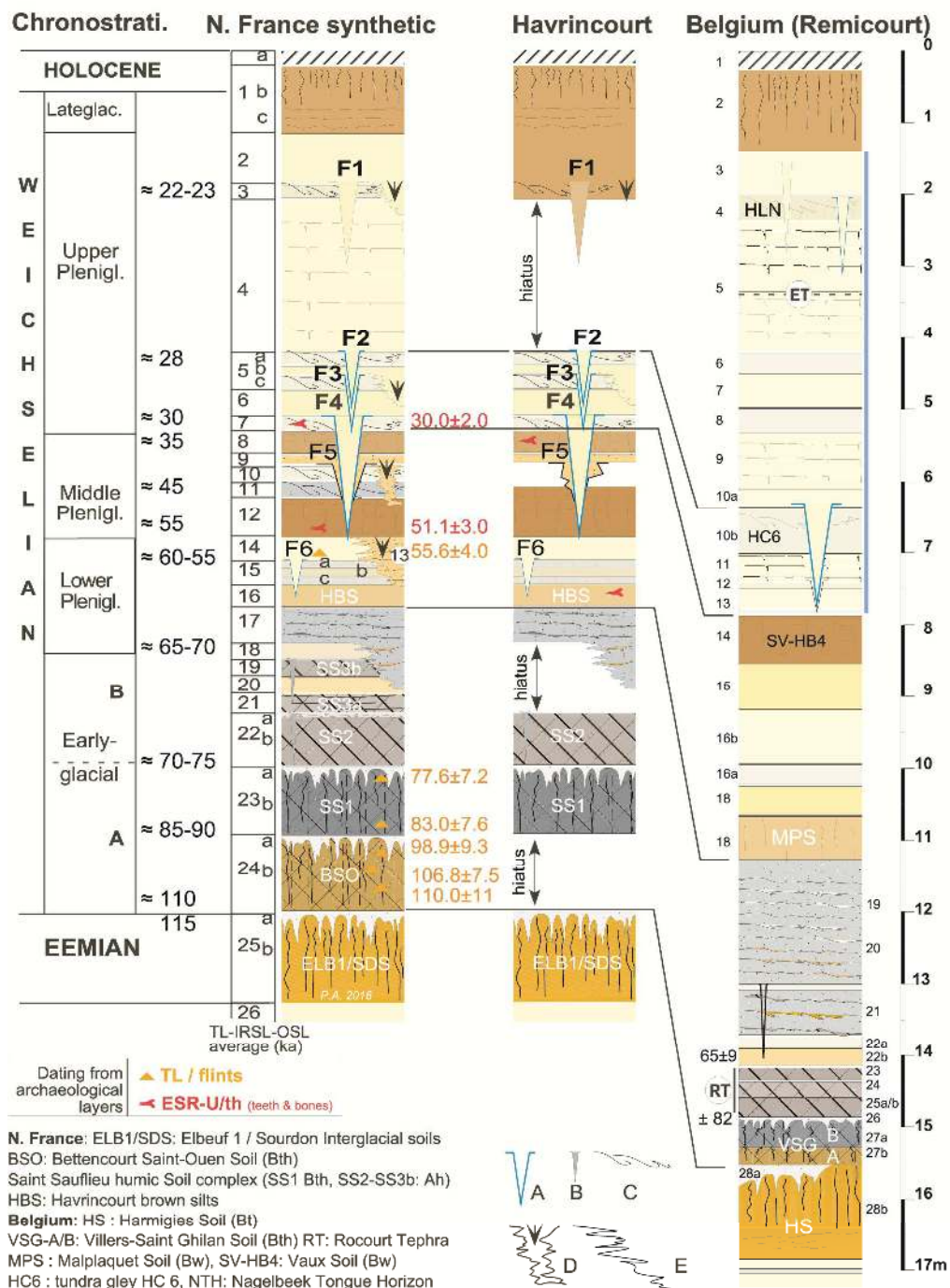
Samples	Unit	Archaeological Level	Tissue	U (ppm)	Equivalent dose D_E (Gy)	U uptake parameter p or n	$D_a \alpha$ Internal ^a ($\mu\text{Gy/a}$)	$D_a \beta$ ($\mu\text{Gy/a}$)	$D_a (\gamma + \text{cosm})^b$ ($\mu\text{Gy/a}$)	D_a total ($\mu\text{Gy/a}$)	ESR/U-series ages (US or AU) ^c (ka)
HAV1201	6a	HAV2-N2	dentine	20.53 ± 0.13	43.15 ± 0.74	-0.9760 ± 0.1715	82 ± 50	147 ± 23	1040 ± 55	1269 ± 78	34.0 ± 2.0
			enamel	0.44 ± 0.01							
HAV1202	12	HAV2-N1	dentine	17.15 ± 0.09	129.02 ± 2.75	-0.0042 ± 0.0008	745 ± 110	178 ± 17	1003 ± 50	1926 ± 122	67.0 ± 4.0
			enamel	3.95 ± 0.02							

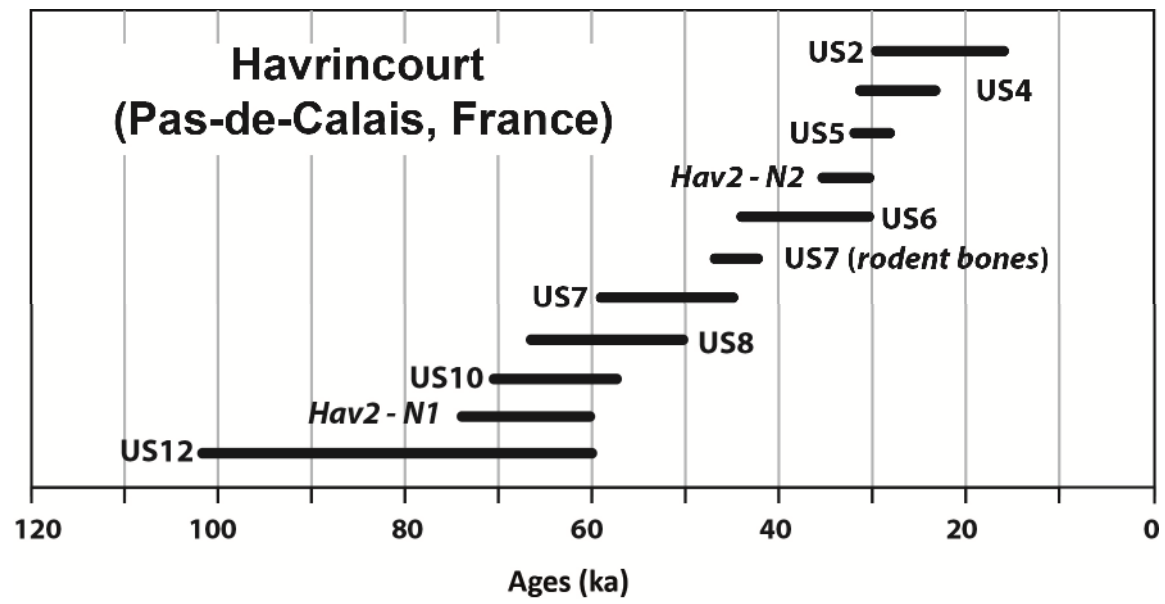
Table 7. ESR/U-series age results for the Havrincourt horse teeth. (a) A k -value of 0.13 ± 0.02 was used according to Grün & Katzenberger-Appel (1994); (b) Cosmic dose was estimated from the Prescott & Hutton's data (1994); (c) Uncertainties on the ESR/U-series ages (model US, Grün et al. 1988 or model AU, Shao et al. 2012) were calculated using Monte-Carlo approach (Shao et al., 2014).

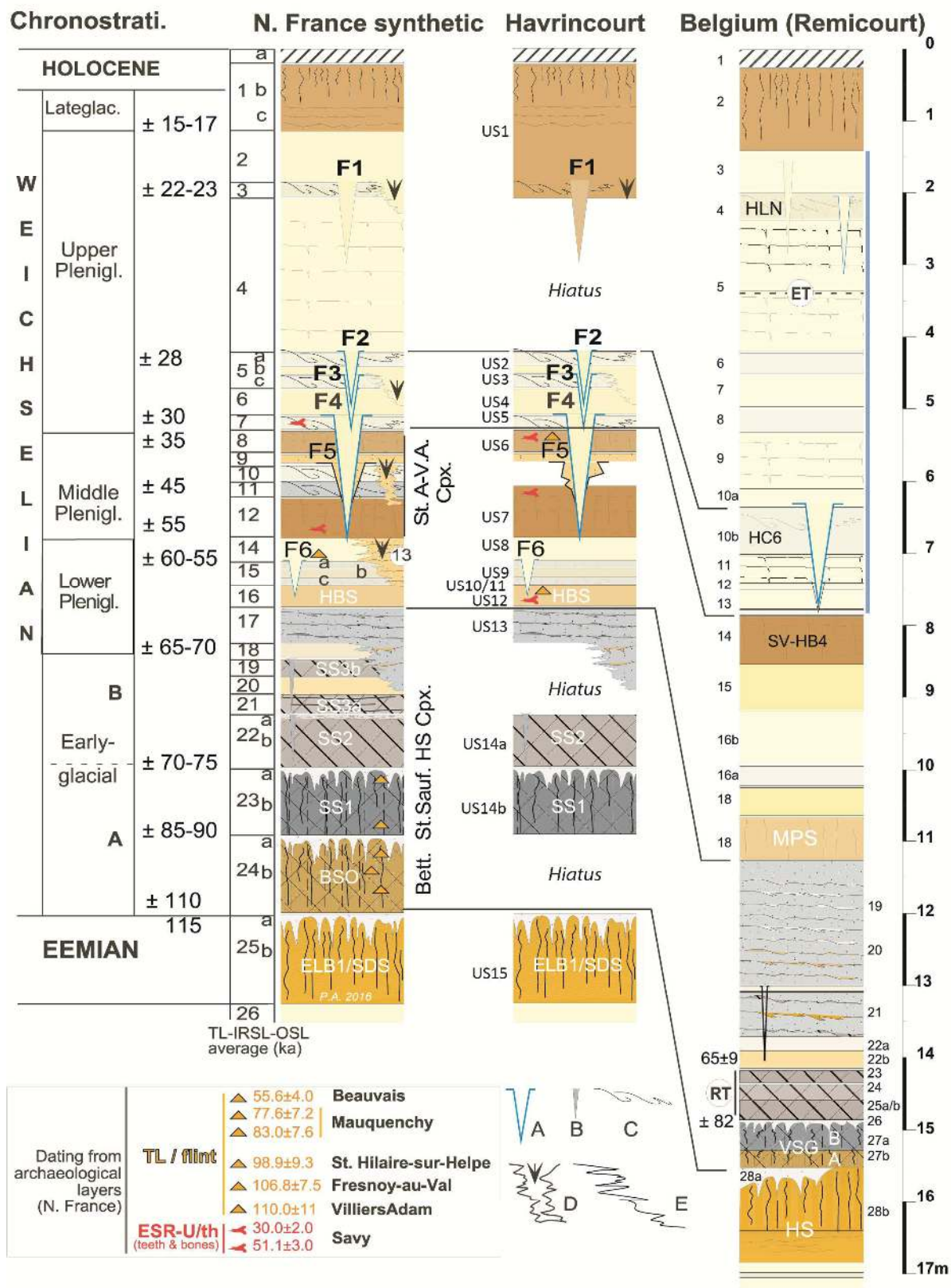
Stratigraphical units	Time Range lower bound	Time Range upper bound
US2	-29 361	-16 217
US4	-31 112	-23 442
US5	-31 548	-28 301
<i>Hav2-N2 archaeological level</i>	-36 887	-30 311
US6	-43 905	-30 528
<i>US7 (rodents bones)</i>	-46 712	-42 354
US7	-58 954	-45 005
US8	-66 263	-50 389
US10	-70 235	-57 620
<i>Hav2-N1 archaeological level</i>	-74 393	-60 937
US12	-101 611	-60 315

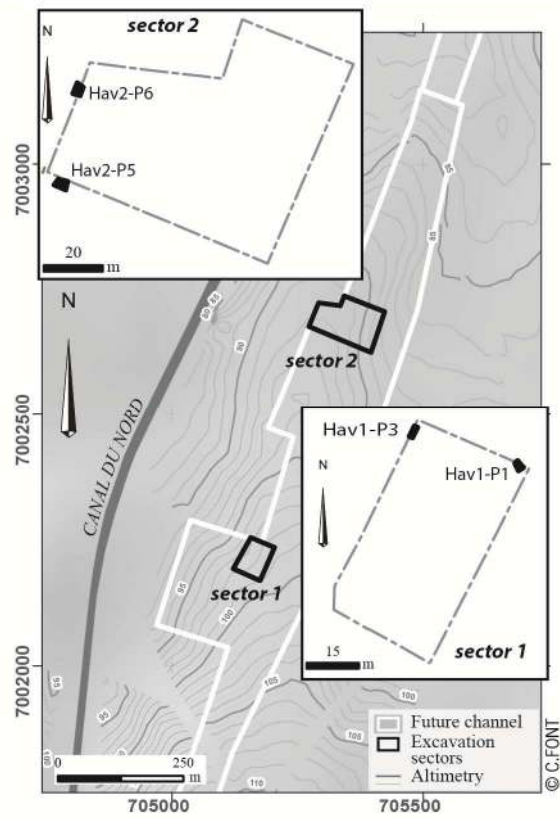
Table 8. Time range endpoints for Havrincourt units (at level 95%). Results are represented in years before 2016 AD.



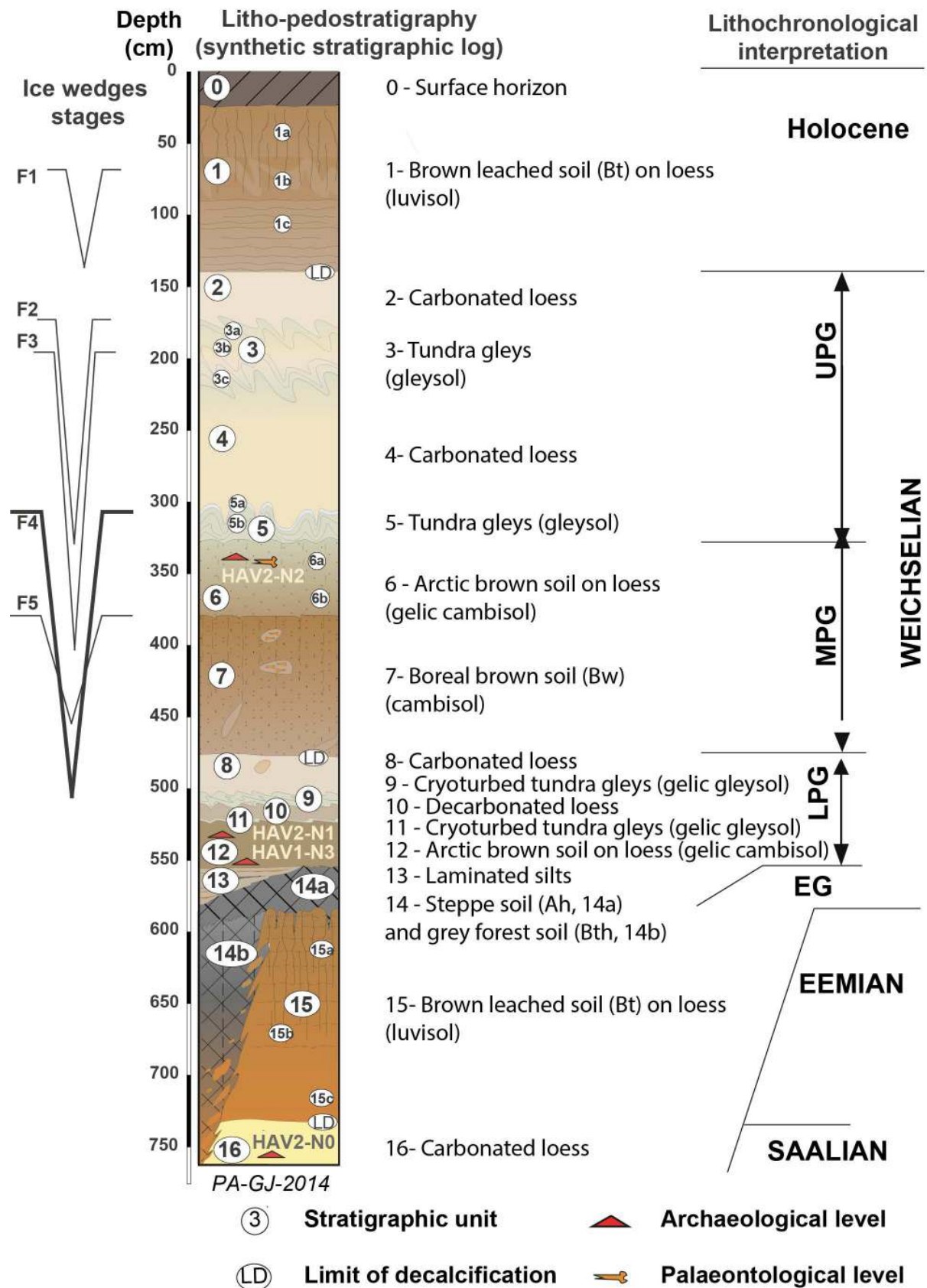


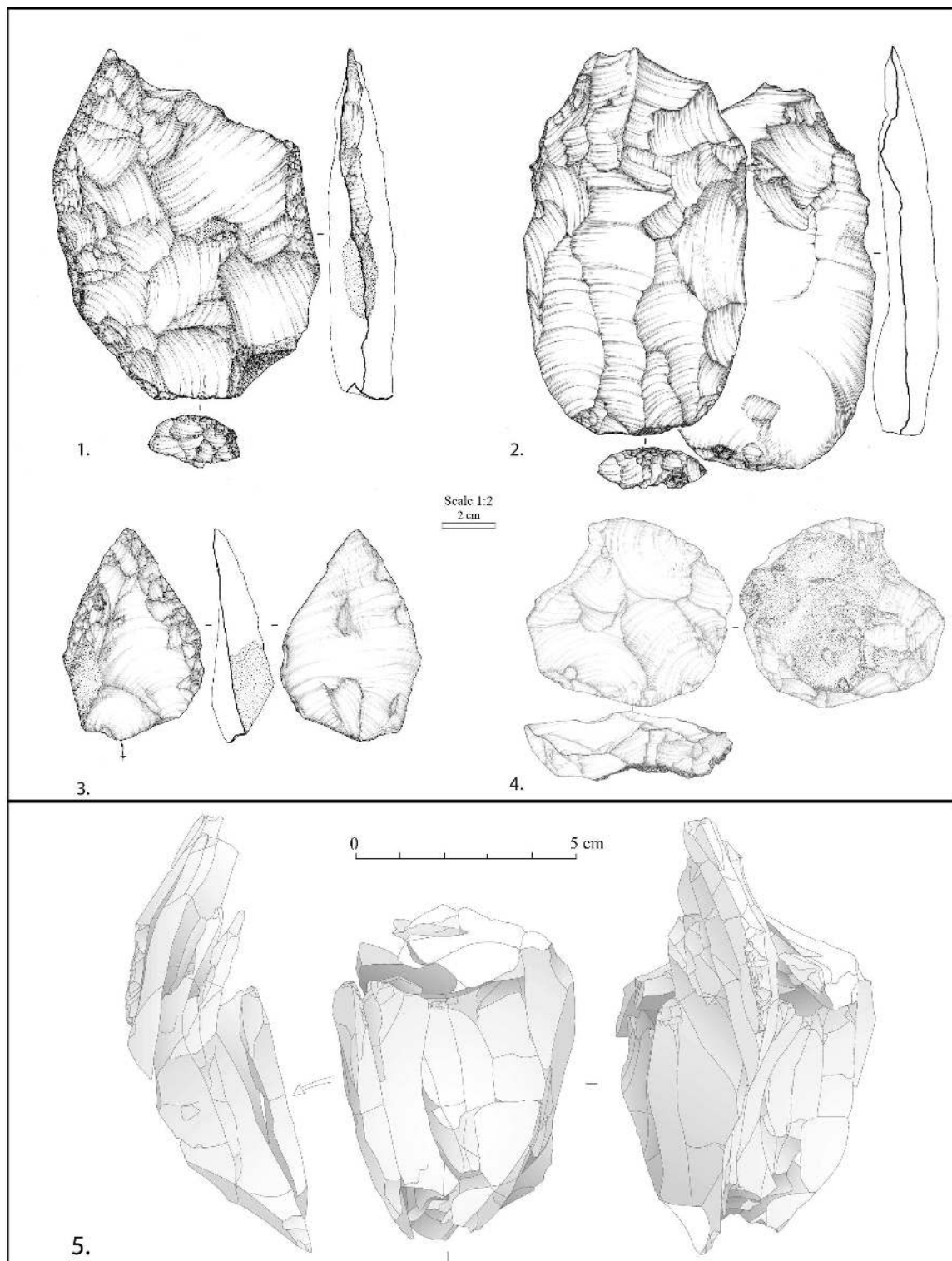






Havrincourt (Pas-de-Calais, France)





Havrincourt (Pas-de-Calais, France)

